PHYSICAL REVIEW D **85,** 035005 (2012)

Probing light stop pairs at the LHC

Xiao-Jun Bi,[1] Qi-Shu Yan,[2] and Peng-Fei Yin[1]

[1]*Laboratory of Particle Astrophysics, Institute of High Energy Physics, Chinese Academy of Sciences, Beijing 100049, China*
[2]*College of Physics Sciences, Graduate University of Chinese Academy of Sciences, Beijing 100049, China*

(Received 6 December 2011; published 7 February 2012)

In this work, we study the light stop pair signals at the LHC. We explore the supersymmetry parameter space with nonuniversal gaugino and third-generation masses at the grand unified theory scale. Recent LHC supersymmetry search results based on 35 pb^{-1} and 1 fb^{-1} of data are implemented to put the limits on stop pair events. The dark matter relic density and direct detection constraints are also taken into account. Detailed simulations on the signals and background for some benchmark points are performed, and it is found that the stop pair signals usually escape the LHC search if the present cut conditions are used. We also explore the potential and sensitivity of ILC to probe such scenarios. It is found that the ILC can detect them with an integrated luminosity of a few tens of fb^{-1}.

DOI: 10.1103/PhysRevD.85.035005 PACS numbers: 12.60.Jv, 14.80.Ly

I. INTRODUCTION

Supersymmetry (SUSY) is one of the most attractive extensions beyond the standard model (SM) which offers a solution to the hierarchy problem and grand unification in gauge interactions. Moreover, the R-parity conserved SUSY models naturally provide a lightest supersymmetric particle (LSP) which is neutral and stable and can be a dark matter candidate badly needed in order to interpret the cosmological observations. To guarantee the electroweak symmetry breaking naturally, the size of SUSY soft breaking terms is believed to be of the electroweak scale, of which the light Higgs boson mass is typically less than about 140 GeV and the masses of sparticles are around a few hundred GeV, which are within the reach of LHC. The running of LHC can test supersymmetry by discovering a light Higgs boson and SUSY particles.

Search for supersymmetry is one of the prime targets of LHC. Certainly the strong interaction sector of the SUSY models is the most important place to discover SUSY due to the large cross sections for the production of colored particles, such as squarks and gluinos, at the hadron colliders. As one of the typical signatures of such processes, the LSPs appearing in the final states lead to a large missing energy (experimentally a large missing transverse momentum). Therefore, SUSY signatures should show up best in the jets plus large missing energy channel. Currently, the most stringent bound is derived from this channel, which is the dominant signature for gluino and squark production. With 1 fb^{-1} of data at the LHC, no SUSY signatures are detected. The bound on the gluino and squark masses are set to be larger than about 800 GeV for the minimal supergravity (mSUGRA) model [1,2]. The recent release of LHC measurements motivated quite a few new works on SUSY [3], where the implications of CMS and ATLAS results to various SUSY models are discussed.

If nature chooses SUSY as its working principle, the null results in the supersymmetric searches at hadronic colliders (both Tevatron and LHC) may indicate that SUSY hides from our probe in some ways. For example, one way is that the SUSY might be splitting in its color sector, i.e., color sparticles are very heavy (say more than a few TeV) and their cross sections are highly suppressed by masses. Then SUSY can only show up at LHC via processes from its electroweak sector. In order to find SUSY, we have to accumulate more data. In some worse cases, SUSY may even be missed at LHC. For example, near degeneracy of the masses of chargino and neutralino leads to soft leptons which can escape the detection at LHC [4]. If this is the case, a linear electron-positron collider or a muon collider will be necessary to unravel such a scenario.

Another possible way is that the SUSY signature is buried deeply in the background events and cannot be selected out with the current search approach. For example, in the compressed SUSY models [5,6], where the mass difference between the squark and LSP is small, only few soft jets can show up in the final states. Thus the signature is so similar to the background events that the currently SUSY search selection conditions cannot separate the signal events.

The scenarios in which gluino and squarks of the third generation are light but degenerate with LSP may also be hidden to the LHC search [7–9]. One such possibility is the light stop scenario [10–27]. The stop can be the next-to-lightest supersymmetry particle (NLSP), which can be quite naturally realized in SUSY models, like mSUGRA. The large top Yukawa coupling has a twofold effect on the stop quark mass spectra. First, the off-diagonal trilinear term, which is proportional to top Yukawa coupling, can lead to the largest mass splitting in the squark sector and consequently produce a light stop as the NLSP. Second, since the lightest stop is mostly right-handed, the mass of the right-handed stop, $m_{\tilde{t}_R}$, is significantly reduced by the top Yukawa coupling via the renormalization group running. Light stop scenario is also well-motivated to explain the dark matter relic density measured by WMAP when the

mass splitting between it and the dark matter candidate (the LSP) neutralino (χ_1^0) is small enough [13]. Such a case is also dubbed as the stop-neutralino coannihilation scenario. Furthermore, the electoweak baryogensis in the framework of the minimal supersymmetric standard model favors a light stop [11,12], i.e., the light stop can generate the first-order phase transition, which prevents the baryon asymmetry of the Universe from being washed out. In order to guarantee this first-order phase transition, the mass of the light stop should be light.

In the mSUGRA scenario, all the gaugino and scalar masses are usually assumed universal at the GUT scale. However, such an assumption is not guaranteed by symmetry. If the F-term of the gauge kinetic function in the $SU(5)$ SUSY GUT is not singlet, the gaugino masses at GUT would not be universal [28,29]. The nonuniversal gaugino masses can also be predicted in the supersymmetric $SU(5) \times SU(3)_{\text{Hypercolor}}$ model proposed to solve the Higgs doublet-triplet splitting problem in $SU(5)$ GUT [30,31], and in the supersymmetric partial unified model $SU(4)_C \times SU(2)_L \times SU(2)_R$ [32]. For the scalar sector, notice the most stringent constraints on SUSY flavor changing neutral current (FCNC) and CP violation processes only relate to the first two generations of sfermions, it is well-motivated to consider the so-called ''inverted scalar mass hierarchy'' scenario [33–36]. In such a scenario, the large masses of the first two generations of sfermions can solve the SUSY flavor and CP problems, while the third-generation sfermions are still light to satisfy the naturalness conditions. These nonuniversal soft breaking parameters will change the running behavior of the renormalization group equation (RGE), and induce different sparticle mass spectra and search strategies from the mSUGRA.

In this work, we will study a SUSY scenario with nonuniversal gaugino and third-generation masses at the GUT scale, and then explore the signatures of the light stop pair production (for some relevant studies, see [37–42]). We first scan the SUSY parameter space in the nonuniversal SUSY model. We have considered all the constraints on the SUSY parameter space. Presently, 1 fb^{-1} of LHC data at ATLAS and CMS are used to put limits on stop pair events. We also simulate the signatures in some benchmark points at the LHC in detail. In general, the stop pair productions depend on stop mass parameter, while the light stop decay modes only rely on light slepton, chargino and neutralino mass spectra. Our results can be easily extended to the scenarios with decoupled gluino and the first two generations of squarks. For the stop-neutralino coannihilation scenario to give correct dark matter relic density, we find the SUSY signatures are hidden by the present cut conditions. We further present a study of the signals at the future linear collider machine.

This paper is organized as follows. In Sec. II, we start with the generic bounds on SUSY from LEP, Tevatron, and LHC, while we concentrate on the bounds to the light stop from its various decay channels searched by experiments. In Sec. III, we analyze the dark matter bounds to the parameter space of nonuniversal SUSY models and study the mass spectrum. In Sec. IV, we discuss the recent LHC bounds for our light stop scenario, and select four benchmark points, demonstrate their mass pattern and decay features, and elaborate how the signature from these benchmark points can hide from the current search at LHC. We also study the sensitivity of ILC to these benchmark points. Section V is for discussions and conclusions.

II. CURRENT EXPERIMENTAL BOUNDS ON LIGHT STOP SCENARIO

In this section we describe the available bounds from the stop pair search at LEP, Tevatron and LHC in detail. Several stop decay modes are investigated in [43], i.e., 1) $\tilde{t} \to \chi_1^+ b$, 2) $\tilde{t} \to \tilde{\nu}\ell b$, 3) $\tilde{t} \to \tilde{\ell}^+ \nu b$, and 4) $\tilde{t} \to \chi_1^0 c$. The recent bounds listed below depend on the mass spectrum and the decay mode of the sparticles.

(i) $\tilde{t}_1 \to b\chi^+ \to b\ell\nu\chi_1^0$: The pair production of stop decaying via $\tilde{t}_1 \to b\chi^+$ has been investigated by the CDF collaboration with an integrated luminosity of 2.7 fb^{-1} [44]. The stop masses between 128 and 135 GeV are excluded at 95% independent of the branching ratio of $\chi^+ \to \ell\nu\chi_1^0$. For $m(\tilde{\chi}_1^0) = 45\,\text{GeV}$, $m(\chi_1^\pm) = 125.8\,\text{GeV}$ and $\text{Br}(\chi^+ \to \ell\nu\chi_1^0) = 1$, a lower limit for stop mass can be set at 196 GeV.

(ii) $\tilde{t}_1 \to b\ell\tilde{\nu}$: The most stringent bounds for stop pair production with this decay channel are given by the D0 collaboration [45] with an integrated luminosity of 5.4 fb^{-1}. The main final states are focused on $b\bar{b}e^\pm\mu^\mp\tilde{\nu}\bar{\tilde{\nu}}$. The sneutrino is assumed to be the LSP or to decay invisibly into $\nu\tilde{\chi}_1^0$. The analysis is optimized for the mass region $\Delta m = m_{\tilde{t}_1} - m_{\tilde{\nu}} = 40$ GeV or above. Stop masses up to 240 GeV are excluded for sneutrino masses around to 45 GeV, and sneutrino masses up to 120 GeV are excluded for stop masses around to 180 GeV.

(iii) $\tilde{t}_1 \to t\chi_1^0$: The recent search for the top partner T' (it can be the t' of the fourth-generation model, the new heavy quark in the little Higgs model with T-parity, or the scalar top quark in the SUSY model) and $T' \to t\chi$ via the semileptonic mode $pp \to \ell\nu_\ell bqq'b + \chi\chi$ and full-hadronic final states $pp \to q_1q_2bq_3q_4b + \chi\chi$ by the CDF collaboration are reported in Refs. [46,47], with integrated luminosities of 4.8 fb^{-1} and 5.7 fb^{-1} respectively. It is shown that the mass of T' can be bound up to 360 GeV for $m_\chi < 100$ GeV and 400 GeV for $m_\chi \leq 70$ GeV, respectively. When both top quarks decay semileptonically, the final states are the same as the first two decay modes, i.e., $\tilde{t}_1 \to b\chi^+$ and $\tilde{t}_1 \to b\ell\tilde{\nu}$. The discovery of this

decay channel with both the discovery hadronic and semileptonic channels can distinguish this decay mode from the others.

(iv) $\tilde{t}_1 \to c\chi_1^0$: If the above processes are all kinetically forbidden, the loop-induced flavor-changing process $\tilde{t}_1 \to c\chi_1^0$ might be the dominant decay channel. The similar process $\tilde{t}_1 \to u\chi_1^0$ is always suppressed by the Cabibbo-Kobayashi-Maskawa matrix when $\tilde{t}_1 \to c\chi_1^0$ kinematically opens. This channel is difficult detect if the mass splitting between $\tilde{t}_1$ and χ_1^0 is smaller, which leads to two soft jets in the final states. The CDF collaboration had performed the research for this process with 2.6 fb^{-1} of data [48]. At least one of the jets is required to be tagged from a heavy-flavor quark. The analysis is optimized for the mass region $\Delta m = m_{\tilde{t}_1} - m_{\tilde{p}} = 40$ GeV or above. Stop masses up to 180 GeV are excluded for neutralino masses around to 95 GeV. In addition, the results from LEP had excluded stop masses up to 90 GeV for $\tilde{t}_1 \to c\chi_1^0 = 1$. A more recent experimental search at D0 collaboration can be found in [49].

(v) $\tilde{t}_1 \to bff'\chi_1^0$: For small mass splitting between stop and the LSP, the four-body process $\tilde{t}_1 \to bff'\chi_1^0$ could be also important [50]. Typically, the objects in this channel are softer comparing with those from $\tilde{t}_1 \to t\chi_1^0$.

(vi) R-hadron: If the lifetime of stop is long enough due to the extremely small mass splitting or weak interaction between stop and the LSP [15], stop can form a bound state R-hadron in the process of hadronization before its decay. If such R-hadron carries electric charge, it might be observed in the inner tracker and even outer muon detector. Recently, CMS collaboration reported the limits for R-hadrons from pair production of stable stops based on 1.09 fb^{-1} of data [51]. Lower limit for stop mass can be set at 620 GeV and 515 GeV, corresponding to whether R-hadrons can leave observable signatures at the muon detector or not, respectively. The search strategy of long-lived stops in the minimal supersymmetric standard model is studied at LHC and can be found in the Monte Carlo study in Ref. [17].

III. ANALYSIS OF THE PARAMETER SPACE

A. Theoretical scenarios

In the mSUGRA scenario, all the gaugino masses are set to be universal as $m_{1/2}$ at the GUT scale. However, this is a convenient assumption rather than a theoretical requirement. A nonuniversal gaugino mass sector is well-motivated in many superstring or SUSY GUT models [28,29,37–39]. In the SUSY GUT, if there exists a holomorphic function $f(\Phi)$ in the gauge kinetic function, gauginos will acquire masses via a nonzero F-term of the $f(\Phi)$

$$\int d^2\theta f(\Phi)_{ab} W^a W^b + \text{H.c.} \sim \frac{1}{\Lambda}\langle F(\Phi)\rangle_{ab}\lambda^a\lambda^b, \quad (1)$$

where Φ is a chiral field in the hidden sector related to SUSY breaking, $\langle F(\Phi)\rangle_{ab}$ transforms in the $Adj \otimes Adj$ representation of the underlying gauge group containing gauginos λ^a, λ^b. For $SU(5)$ SUSY GUT, $\langle F(\Phi)\rangle_{ab}$ belongs to $24 \otimes 24 = 1 \oplus 24 \oplus 75 \oplus 200$. Only if $\langle F(\Phi)\rangle_{ab}$ is a singlet as $\langle F(\Phi)\rangle_{ab} \sim c\delta_{ab}$, gaugino masses are universal as in the mSUGRA. The nonuniversalities are generated when $\langle F(\Phi)\rangle_{ab}$ belongs to other high representations. For example, the gaugino mass relationships at GUT scale are $2: -3: -1$, $1:3: -5$ and $1:2:10$ for $f(\Phi)$ belonging to 24, 75, 200 respectively [28,29]. Moreover, if different $f(\Phi)$ representations appear simultaneously, other gaugino mass relations can be achieved.

In the scalar sector, a general Kähler potential could also leads to mass nonuniversality [37,38]

$$\int d^2\theta d^2\bar{\theta} K_0 Q^\dagger Q + K_j^i Q_i^\dagger Q^j + \ldots \sim c_{ij}\phi^i\phi^j, \quad (2)$$

where $K_0, K_j^i, \ldots$ are real function of $\Phi^\dagger$, Φ. In the mSUGRA scenario, all the scalar fields acquire same mass under the universal Kähler potential assumption $K_j^i \sim K\delta_j^i$. This assumption is useful to suppress FCNC effects which are stringently constrained by experiments. However, solving the SUSY flavor and CP problems only requires large masses of the first two generations of sfermions, while the third-generation sfermions can still be light to satisfy the naturalness conditions [33–36].

Therefore, in this work, we treat these soft breaking mass parameters as free parameters at the GUT scale without imposing specific relations among them which can be derived from their underlying nonuniversal models. For the sake of simplicity, we choose the following seven input parameters as free parameters in our analysis:

$$M_{1/2},\quad M_{1/2,3},\quad m_0,\quad m_{0,3},\quad A_0,\quad \tan\beta,\quad \text{sign}(\mu). \quad (3)$$

Compared with mSUGRA, only two extra input parameters at GUT scale, i.e., the gluino mass $M_{1/2,3}$ and the third-generation sfermion mass $m_{0,3}$, are added.

B. Parameter Space Scan and Experimental Constraints

In this subsection we scan the SUSY parameter space with the seven free parameters at the GUT scale discussed above. The low-energy spectra are calculated by solving the RGEs. In the scanning, the GUT and the electroweak symmetry-breaking scale are set to be $M_{\text{GUT}} = 2 \times 10^{16}$ GeV and $M_{\text{EWSB}} = \sqrt{m_{\tilde{t}_1} m_{\tilde{t}_2}}$, respectively. We consider the case where gluino is lighter than wino and bino at M_{GUT} and put a constraint by requiring 100 GeV $< M_{1/2,3} < M_{1/2} < 800$ GeV. To obtain a lighter stop or stau,

which is necessary in order to yield a suitable DM relic density, we further assume that third-generation sfermions are lighter than the other scalars in the first two generations, and allow them to vary in the range $100\ \text{GeV} < m_{0,3} < m_0 < 2000\ \text{GeV}$. The trilinear coupling A_0 and the ratio of vacuum expectation values $\tan\beta$ are chosen in the range of $-1 < A_0/m_0 < 1$ and $2 < \tan\beta < 50$, respectively. The sign of μ is taken to be positive, which is favored by several experimental constraints on $b \to s\gamma$ etc. We utilize SUSPECT [52] to calculate the SUSY particles' spectra by solving the two-loop SUSY renormalization group equations. The top quark pole mass can affect the sparticle spectra and consequently modify dark matter relic density significantly. We take the top pole mass as $m_t(\text{pole}) = 173.1\ \text{GeV}$..

Several phenomenology and astrophysics experimental constrains are taken into account in our scanning. Important flavor physics constraints: $\text{Br}(b \to s\gamma) = (3.55 \pm 0.24) \times 10^{-4}$ [53], $\text{Br}(B_s \to \mu^+\mu^-) = (0 \pm 1.4) \times 10^{-8}$ [54], $\text{Br}(B_u \to \tau\bar{\nu})/\text{SM} = 1.28 \pm 0.38$ [53], are realized. As a conservative analysis, we only demand that the SUSY contributions pass these constraints to a 3σ level. Another remarkably important constraint is from the muon anomalous magnetic moment $g_\mu - 2$ measurement [55], which is adopted here as a bound $-11.4 \times 10^{-10} < g_\mu - 2 < 9.4 \times 10^{-9}$ as used in Ref. [40]. The lighter Higgs boson is required to be heavier than 114 GeV, while the mass limits for other charged sparticles from LEP are also imposed [56].

Constraints by dark matter relic density are also considered. In our analysis, the lightest neutralino is required to be LSP and a candidate of dark matter. The dark matter relic density is reported by WMAP7 in the range $\Omega h^2 = 0.112 \pm 0.0056$ [57]. However, we only require the thermal abundance of neutralino satisfies a 3σ upper bound $\Omega_{\chi_1^0} h^2 < 0.1288$ because the neutralino might not be the only dark matter particle or that the neutralino might be produced in the early Universe via the so-called nonthermal mechanism [58]. The recent direct search experiment XENON100 [59] is realized, which put the most stringent bound upon the dark matter-nucleon spin-independent scattering. We demand that the reduced dark matter-nucleon scattering cross section $\sigma_r^{\text{SI}} = \sigma_{\chi_1^0 p}^{\text{SI}} (\Omega_{\chi_1^0} h^2 / \Omega h^2)$ should be smaller than XENON100 limit. All constraints on flavor physics from low-energy colliders and all bounds on dark matter from astrophysics and direct detection are implemented by using MICROMEGAS [60], which uses the SUSPECT output as input parameters.

C. Numerical results and sparticle masses

In this section, we present some results based on a $\sim 10^6$ case study in our parameter space scan. We find that most of the points cannot yield correct RGE solutions nor induce the spontaneous electroweak symmetry breaking. Only ~ 700 points can pass all the constraints. To analyze the features of dark matter and collider signatures, it is found that light sparticles play the crucial roles. It is convenient to categorize the parameter points in term of the mass hierarchical relation of light sparticles as suggested in Ref. [40]. Here we define our four mass patterns:

(1) the stop pattern (SO): $m_{\chi_1^0} < m_{\tilde{t}_1}, m_{\chi_1^\pm}$;
(2) the stau/stop pattern (SS): $m_{\chi_1^0} < m_{\tilde{\tau}_1} < m_{\tilde{t}_1} < m_{\chi_1^\pm}$;
(3) the stau pattern (SA): $m_{\chi_1^0} < m_{\tilde{\tau}_1} < m_{\chi_1^\pm} < m_{\tilde{t}_1}$;
(4) the chargino pattern (CH): $m_{\chi_1^0} < m_{\chi_1^\pm} < m_{\tilde{\tau}_1}, m_{\tilde{t}_1}$.

In Fig. 1, we present two scattering plots to reveal some features of these four mass patterns. In plot (a), points are shown in the $m_{\chi_1^0} - m_{\tilde{t}_1}$ plane. In plot (b), they are shown in $m_{\chi_1^\pm} - m_{\tilde{t}_1}$ plane. The distribution of these four mass patterns in soft SUSY-breaking parameter space are also shown in Fig. 2. In Fig. 2(a)–2(d), the distribution on the $m_0 - M_{1/2}$ plane, on the $m_{0,3} - M_{1/2,3}$ plane, on the $A_0 - \tan\beta$ plane, and on the $M_1 - \mu$ plane are displayed,

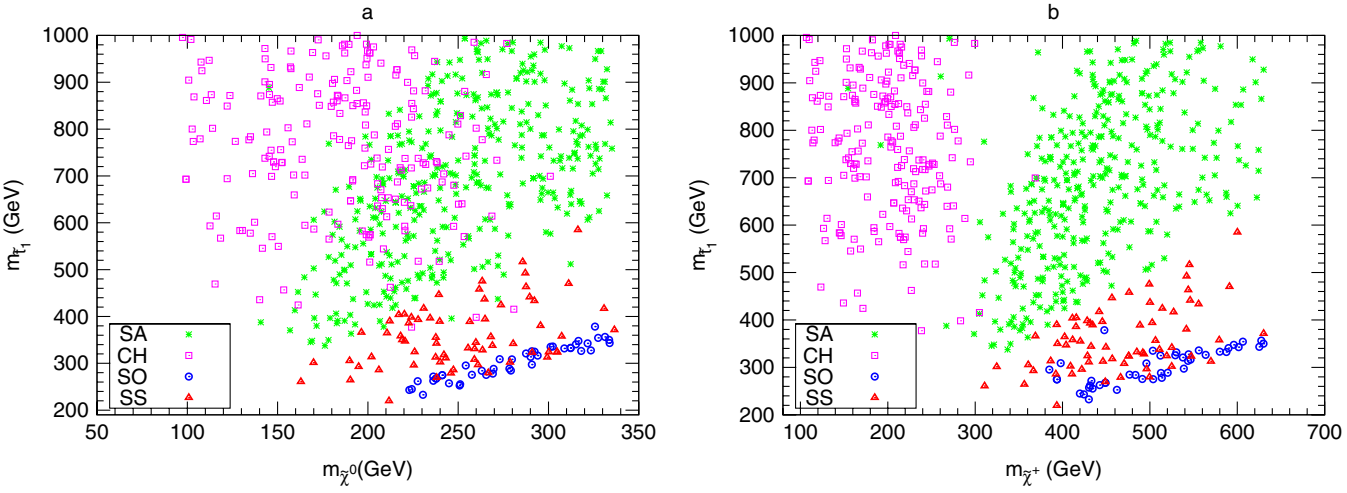

FIG. 1 (color online). Four mass patterns in the planes (a) $m_{\chi_1^0}$ vs $m_{\tilde{t}_1}$ (top left), (b) $m_{\chi_1^\pm}$ vs $m_{\tilde{t}_1}$ (top right) are illustrated.

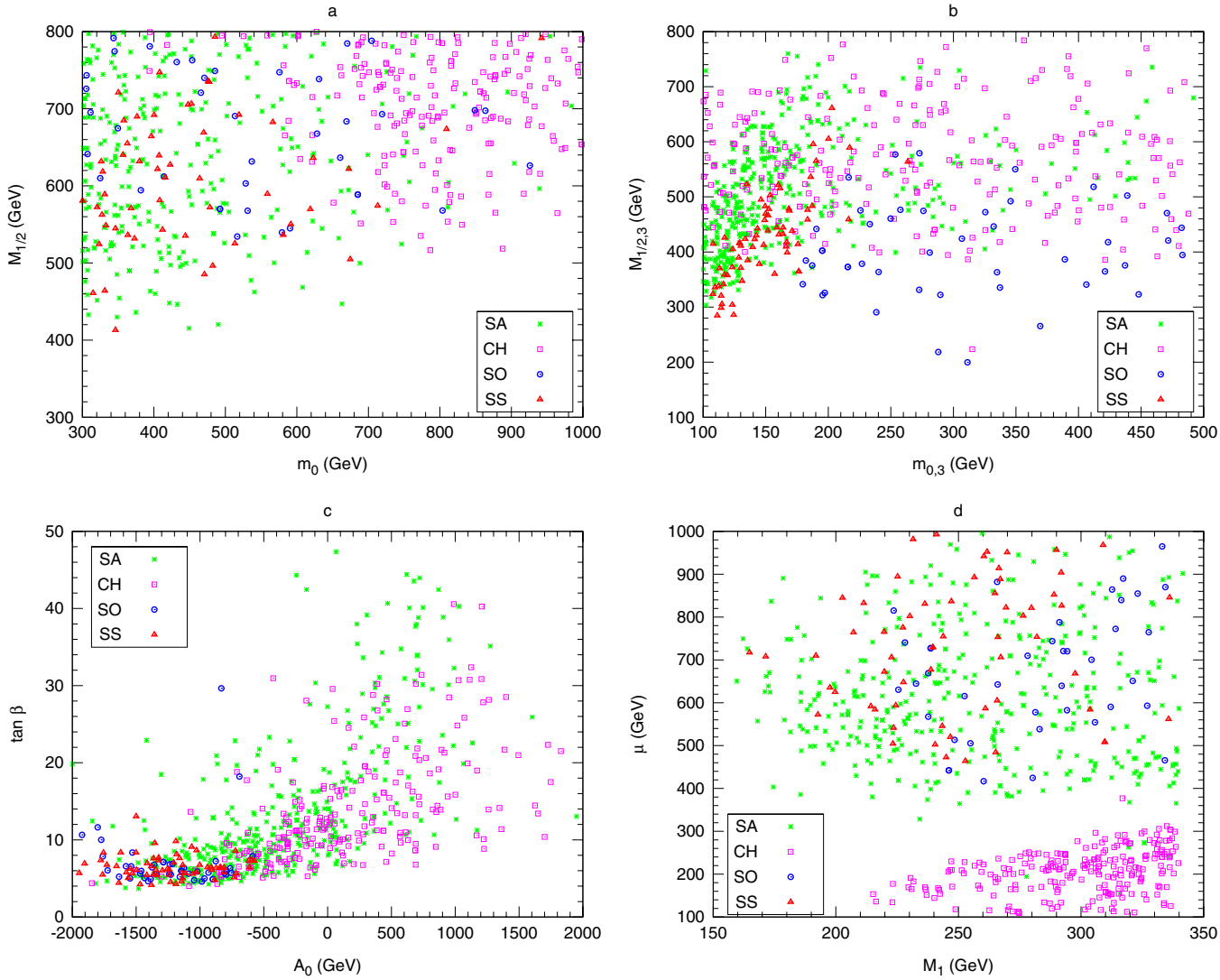

FIG. 2 (color online). Four mass patterns in the planes (a) m_0 vs $M_{1/2}$ (top left), (b) $m_{0,3}$ vs $M_{1/2,3}$ (top right), (c) A_0 vs tanβ (bottom left), (d) M_1 vs μ (bottom right) are displayed, respectively.

respectively. Four comments on the distributions are listed in order:

(1) The gaugino mass running behavior in the nonuniversal scenarios is similar to that in mSUGRA. The one-loop RGEs for gaugino masses are

$$16\pi^2 \frac{d}{dt} M_i = 2 b_i g_i^2 M_i, \tag{4}$$

where $(b_1, b_2, b_3) = (33/5, 1, -3)$. It is well-known that in the mSUGRA the soft breaking parameters $M_3^0 = M_2^0 = M_1^0$ at $M_{\rm GUT}$ evolves to $M_3{:}M_2{:}M_1 \sim \alpha_3 M_3^0{:}\alpha_2 M_2^0{:}\alpha_1 M_1^0 \sim 6M_3^0{:}2M_2^0{:}M_1^0$ at M_Z. In the nonuniversal scenarios, gaugino mass parameters of first two generations at low energy hold this relation $M_1{:}M_2 \sim 1{:}2$, which consequently means that the main component of the lightest neutralino $\tilde{\chi}_1^0$ is either bino or Higgsino, depending on the relations of M_1 and μ. This $M_1 - M_2$ relation also implies the lighter chargino $\tilde{\chi}_1^+$ and the next lightest neutralino $\tilde{\chi}_2^0$ should almost degenerate, since both of them are $SU(2)$ gaugino dominant $m_{\tilde{\chi}_1^+} \sim m_{\tilde{\chi}_2^0} \sim M_2$. In the Fig. 1(a) and 1(b), we can observe that the $m_{\tilde{\chi}_1^0}$ and $m_{\tilde{\chi}_1^+}$ vary in the region of $\sim$(100, 350) GeV and (100, 700) GeV, respectively, which basically reflects such a relation. On the other hand, the gluino mass parameter M_3 gains a large contribution via a negative β function at low energy, which leads to large gluino mass. It is beyond the reach of Tevatron, or even the reach of LHC with $\sqrt{s} =$ 7 TeV if gluino mass is heavier than 1 TeV.

(2) The one-loop RGEs for the third-generation right-handed sfermion squared-mass parameter could be written as

$$16\pi^2\frac{d}{dt}m^2_{\tilde{u}_3} = 4y_t^2(m^2_{H_u}+m^2_{Q_3}+m^2_{\tilde{u}_3}) - \frac{32}{3}g_3^2|M_3|^2 - \frac{32}{15}g_1^2|M_1|^2 + 4|A_tY_t|^2 - \frac{4}{5}g_1^2S, \quad (5)$$

$$16\pi^2\frac{d}{dt}m^2_{\tilde{d}_3} = 4y_b^2(m^2_{H_d}+m^2_{Q_3}+m^2_{\tilde{d}_3}) - \frac{32}{3}g_3^2|M_3|^2 - \frac{8}{15}g_1^2|M_1|^2 + 4|A_bY_b|^2 + \frac{2}{5}g_1^2S, \quad (6)$$

$$16\pi^2\frac{d}{dt}m^2_{\tilde{e}_3} = 2y_\tau^2(m^2_{H_d}+m^2_{L_3}+m^2_{\tilde{e}_3}) - \frac{24}{5}g_1^2|M_1|^2 + 2|A_\tau Y_\tau|^2 + \frac{6}{5}g_1^2S, \quad (7)$$

where S is defined as $S = \mathrm{Tr}[Y_i m^2_{\phi_i}]$. For the first two generations ofsfermions, the terms proportional to Yukawa couplings can be neglected due to the tiny values of their Yukawa couplings. In contrast, the sfermion mass terms of the third generation can get a large contribution from the Yukawa coupling terms. Therefore, a light stop is often the lightest squark due to its large Yukawa couplings. When compared with mSUGRA, the assumption $m_{0,3} < m_0$ is can further decrease the contribution of gluino to the squark mass parameters. This can be read out from Fig. 2(b), where typically our stop pattern corresponds to a smaller value in $m_{0,3}$ parameter. The lightest squark being the lighter stop means that its cross section can be the largest at the hadronic colliders, Tevatron and LHC. The mass relation between stop and stau is difficult to read out from RGE. Typically, the $m^2_{\tilde{\tau}}$ gets less positive contributions from gauginos and the Yukawa coupling Y_τ is much smaller than Y_t as well, which leads to quite a few mass patterns of light third-generation sfermions.

(3) The one-loop RGE for the Higgs mass parameters H^2_u is given as

$$16\pi^2\frac{d}{dt}m^2_{H^2_u} = 6y_t^2(m^2_{H_u}+m^2_{Q_3}+m^2_{\tilde{u}_3}) - 6g_2^2|M_2|^2 - \frac{6}{5}g_1^2|M_1|^2 + 6|a_t|^2 + \frac{3}{5}g_1^2. \quad (8)$$

The $m^2_{H_u}$ evolves to be negative at the low scale due to the large terms proportional to Y_t^2, which is essential in order to induce a spontaneous electroweak symmetry breaking. In the nonuniversal scenario, a smaller third-generation sfermion mass leads to a $|m^2_{H_u}|$ smaller than its counterpart in the mSUGRA. A small $|m^2_{H_u}|$ can lead to a small soft Higgs mass parameter μ, due to the fact that μ is determined by the $m^2_{H_u}$ from the tree- level relation

$$\mu^2 = \frac{m^2_{H_u}\sin^2\beta - m^2_{H_d}\cos^2\beta}{\cos 2\beta} - \frac{m_Z^2}{2}. \quad (9)$$

When the magnitude of μ is comparable to that of M_1, as demonstrated in the cases of CH patten, the lightest neutralino $\tilde{\chi}^0_1$ can have a large component of Higgsino due to the large mixing.

(4) The squared-mass matrix for the stop quark in the weak interaction eigenstate basis $(\tilde{t}_L, \tilde{t}_R)$ is given by

$$\begin{pmatrix} m^2_{Q_3}+m_t^2+\Delta_{\tilde{u}_L} & v(a_t^*\sin\beta - \mu y_t\cos\beta) \\ v(a_t\sin\beta - \mu^* y_t\cos\beta) & m^2_{\tilde{u}_3}+m_t^2+\Delta_{\tilde{u}_R} \end{pmatrix}, \quad (10)$$

where $\Delta_{\phi_i} = (T_{3\phi} - Q_\phi \sin^2\theta_W)\cos(2\beta)m_Z^2$, and $a_t = A_tY_t$. The off-diagonal elements can generate a large mass split between two stop mass-eigenstates, which are labeled as $(\tilde{t}_1, \tilde{t}_2)$. For the case $\mathrm{sign}(\beta) > 0$ chosen in this study, a small $tg\beta$ and a large $-a_t$ can produce a large mass splitting and leads to a relatively lighter stop $\tilde{t}_1$, which is reflected in Fig. 2(c). In contrast, if the a_t is positive and the μ is small, $m_{\tilde{t}_1}$ might be not light when compared with $m_{\tilde{\chi}_+}$, which leads to the cases of the CH patten.

D. Features of the dark matter

In SUSY models, most parameter space leads to a neutralino relic density which is too large to overclose the Universe. Depending on the mass spectra, four working processes can be introduced to produce a small relic density of neutralino [61]:

(1) all the sfermions are light, neutralinos annihilate via t-channel sfermions exchange;
(2) $\tilde{\chi}^0_1$ has a significant component of Higgsino or wino, main annihilating channel is to gauge bosons or Higgs;
(3) neutralinos scatter with sfermions with nearly mass degeneracy which is so-called ''coannihilation'';
(4) neutralinos annihilate via s-channel Higgs resonance with $2m_{\tilde{\chi}^0_1} = m_{A^0}$, or m_{h^0}, m_{H^0}.

When the stop $\tilde{t}_1$ is light, two main processes can lead to a small neutralino abundance. The first is the neutralino-stop coannihilation process $\tilde{\chi}^0_1\tilde{t}_1 \to tg/h_0$, and the other is $\tilde{\chi}^0_1\tilde{\chi}^0_1 \to t\bar{t}$ by the t-channel via exchanging the light stop when the kinematic is allowed. When the lighter stau $\tilde{\tau}_1$ is light, the neutralino-stau coannihilation can occur and make dominant contribution. This is the case with SA and SS. It is worthwhile mentioning that the neutralino-stop coannihilation can be significant for the case of SS.

For the case of CH, the lightest neutralino $\tilde{\chi}^0_1$ has a large component of Higgsino due to the large mixing deduced by the small μ and the large m_0, as shown in the Fig. 2. Two dominant annihilation processes can occur. (1) The pair of

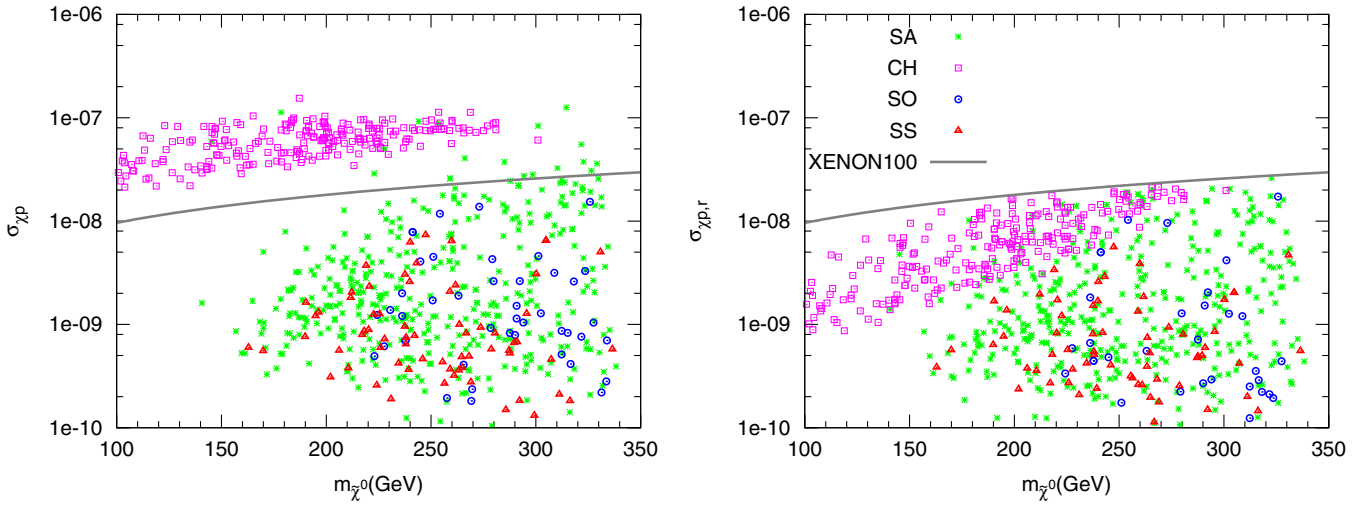

FIG. 3 (color online). The elastic spin-independent DM-nucleon cross section $\sigma_{\tilde{\chi}_1^0 p}$ (left panel) and reduced cross section $\sigma_{\tilde{\chi}_1^0 p,r}$ (right panel) for our four mass patterns are.

neutralinos can annihilate into gauge boson and Higgs boson via the processes $\tilde{\chi}_1^0\tilde{\chi}_1^0 \to W^+W^-$, ZZ, Zh_0 due to large Higgsino component. (2) A neutralino and a chargino can coannihilate into the particles of the SM via the processes $\tilde{\chi}_1^0\tilde{\chi}_1^\pm \to W^\pm Z/\gamma$, $f\bar{f}'$, which can occur due to the small chargino mass and a large Higgsino component in chargino $\tilde{\chi}_1^\pm$.

Last but not least, the sfermion-sfermion self-annihilation processes may also be important, which can be attributed to the fact that a large sfermion-sfermion self-annihilation can increase the effective total dark matter cross section when the mass splitting between sfermion and neutralino is small. Such a case can happen, as we can read out from the effective cross section at the dark matter frozen-out epoch [62]

$$\sigma_{\text{eff}} = \Sigma_{ij;kl}\sigma_{ij;kl}r_i r_j,$$
$$r_i = \frac{n_{eq}^i}{n_{eq}} = \frac{g_i}{g_{\text{tot}}}(1+\Delta_i)^{3/2}\exp(-\Delta_i m_{\tilde{\chi}_1^0}/T), \qquad (11)$$

where Δ_i is defined as $\Delta_i = (m_i - m_{\chi_1^0})/m_{\tilde{\chi}_1^0}$.

The neutralino-nucleon spin-independent scattering can be detected by dark matter direct search through $\tilde{\chi}_1^0 q \to \tilde{\chi}_1^0 q$ via squark or Higgs exchange. If the first two generations of squarks are light or the neutralino has a large Wino/Higgsino component, the null results from direct detection can put a strong constraint on SUSY models. Recently, the XENON100 collaboration observed three events with an background of 1.8 ± 0.6 after 48 kg $\times$ 100.9 days running [59]. The result can be used to constrain the dark matter-nucleon spin-independent scattering cross section.

We show the neutralino-nucleon cross section $\sigma_{\tilde{\chi}_1^0 p}$ (left panel), the reduced cross section $\sigma_{\tilde{\chi}_1^0 p,r}$ (right panel), and XENON100 limit in Fig. 3. Here the reduced neutralino-nucleon cross section defined as $\sigma_{\tilde{\chi}_1^0 p,r} = \sigma_{\tilde{\chi}_1^0 p}(\Omega_{\chi_1^0}h^2/\Omega h^2)$ takes into account that the neutralino may only contribute part of the total dark matter relic density. From Fig. 3(a), we can observe that the neutralino in the CH case has a large $\sigma_{\tilde{\chi}_1^0 p}$ due to its large Higgsino component. If we assume that the neutralinos are produced by a nonthermal process with a correct relic density $\Omega_{\chi_1^0}h^2 = \Omega h^2$, such a scenario is almost excluded by XENON100. If we assume the neutralino only contributes part of the total dark matter relic density, such a scenario is still allowed, as shown in Fig. 3(b).

IV. THE SIGNATURE OF LIGHT STOP PAIRS AT THE LHC

A. production and decay of stop pairs

In this section, we focus on the production and decays of the lighter top squark at the colliders. As pointed out above, the lighter stop $\tilde{t}_1$ can have a smaller mass than all other colored sparticles in the nonuniversal scenario and the mass splitting between it and the other colored sparticle can reach to 1 TeV. Then it is expected that the cross section of the lighter stop pairs at the LHC should be the largest one in our mass patterns introduced above. A pair of stop can be produced via two main processes via $q\bar{q}$ annihilation and gluon fusion [63]. The first one is dominant at Tevatron while the second is dominant at LHC.

To evaluate the cross section of stop pair production $\sigma_{\tilde{t}_1\tilde{t}_1}$ at hadronic colliders, we utilize the package PROSPINO , which has incorporated the next-leading-order corrections. The results for Tevatron with $\sqrt{s} = 1.98$ TeV, LHC with $\sqrt{s} = 7$ TeV and 14 TeV are plotted in Fig. 4. The K factor is determined to be situated in the range of $\sim(1.0, 1.3)$, $\sim(1.5, 2.0)$ and $\sim(1.5, 1.8)$ for Tevatron, LHC7, and LHC14, respectively.

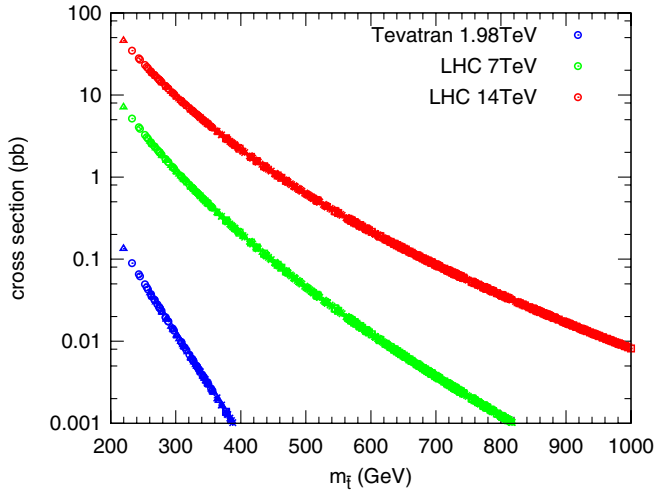

FIG. 4 (color online). The cross sections of stop pair production at Tevatron, LHC-7 TeV and LHC-14 TeV are shown.

In Fig. 4, we observe that the mass of $\tilde{t}_1$ almost monotonically determines the cross section $\sigma_{\tilde{t}_1\tilde{t}_1}$, which is not sensitive to other SUSY parameters. At Tevatron, it is 0.1 pb or so for $m_{\tilde{t}_1} \sim 200$ GeV and quickly decreases to 1 fb when $m_{\tilde{t}_1}$ increases to 400 GeV. At the LHC with $\sqrt{s} = 7$ TeV, the $\sigma_{\tilde{t}_1\tilde{t}_1}$ is larger than its value at Tevatron by a factor of 100 and decreases to 1 fb for $m_{\tilde{t}_1} \sim 800$ GeV. For the $m_{\tilde{t}_1} < 350$ GeV, more than one stop pair events at the LHC7 with 35 pb^{-1} is predicted. With the increasing of $\sqrt{s}$ to 14 TeV and a larger integrated luminosity (say 100 fb^{-1}), stop pair events should be copiously produced when the lighter stop is less than 400 GeV.

In order to analyze the signatures of stop pairs and to reduce the standard model background by setting cuts, we have to study the decay products of stop pair. For this purpose, we use the SDECAY package [65] to compute stop decay branching fractions.

When the lighter stop is much heavier than the LSP, the two-body decay $\tilde{t}_1 \to t\chi^0$ and $\tilde{t}_1 \to b\chi_1^+$ can be its dominant decay modes. In the $\tilde{t}_1 \to b\chi_1^+$ decay mode, the χ_1^+ can mainly decay into $\chi_1^0 W^+$ or $\nu\tilde{\tau}$, which is determined by the mass of stau and the dominant component of χ_1^+. This is the feature of the SA and CH cases. When the lighter stop is smaller than 400 GeV, these two-body decay modes may be forbidden kinematically. Then the three-body decay modes $\tilde{t}_1 \to bW\chi_1^0$ and $\tilde{t}_1 \to \nu\tilde{\tau}\chi_1^0$ become dominant[1] in our scan. When the mass splitting between stop and neutralino is too small to allow the three-body decay, the four-body decay mode $\tilde{t}_1 \to bjj\chi_1^0/b\nu l\chi_1^0$ (a recent study showed that this decay mode can be used to probe trilinear coupling A_0 when tanβ is small [66]) or the loop-induced FCNC decay $\tilde{t}_1 \to c\chi_1^0$ become dominant.

[1]It is necessary to mention that the three-body decay channels $\tilde{t}_1 \to l\tilde{\nu}\chi_1^0$ searched by Tevatron collaborations are not important in our scenario. Since the $m_{\tilde{\tau}}$ is much smaller than $m_{\tilde{\nu}}$, we observe that the branching fraction of $\tilde{t}_1 \to \nu\tilde{\tau}\chi_1^0$ will always be larger than that of $\tilde{t}_1 \to l\tilde{\nu}\chi_1^0$.

B. Simulation and analysis

Recently, CMS and ATLAS collaborations reported several results on their searching for SUSY in different channels. In this section, we present the LHC bounds to the stop pair production with a collision energy $\sqrt{s} = 7$ TeV in terms of different channels studied by CMS and ATLAS.

In our analysis, parton-level events are generated by MADGRAPH [67], while parton shower, decays, and hadronization are performed by PYTHIA [68]. PGS [69] is used to simulate detector effects and to find jets, leptons, and missing transverse momentum. The acceptance cuts for all jets and charge leptons are chosen as $p_t > 20$ GeV and $|\eta| < 2.5$.

The SUSY search strategies of CMS and ATLAS are optimized for mSUGRA scenario at this stage. It always requires large missing transverse energy (MET) and energetic leading jets in order to capture the signature from the heavy squark or gluino pair productions. Therefore the search of the jets plus the MET channel sets the most stringent constraint on ordinary parameter space in mSUGRA. Cuts for studying this channel are described as follows:

(i) In Ref. [1], CMS presents a search for SUSY signatures on an integrated luminosity of 1.14 fb^{-1} with jets and significant MET and without leptons. In this analysis, jets are required

$$E_T^{j_1,j_2} > 100\,\text{GeV}, \quad E_T^{j} > 50\,\text{GeV}, \quad |\eta|_j < 3, \tag{12}$$

where we have used the convention $p_T^{j_i} > p_T^{j_{i+1}}$. The following selections are adopted to compute event rate

$$H_T > 275\ \text{GeV}, \qquad \alpha_T > 0.55, \tag{13}$$

where H_T and α_T are defined as

$$H_T = \Sigma E_T^{j_i}, \qquad H_T = |-\Sigma \vec{p}_T^{\,j_i}| \tag{14}$$

$$\alpha_T = E_T^{J_2}/\sqrt{H_T^2 - \not{H}_T^2}. \tag{15}$$

If the jet number is more than two, we utilize hemisphere algorithm [70] to combine jets into two pseudojets named J_1, J_2 (assumed $p_T^{J_1} > p_T^{J_2}$ again). The events containing isolated leptons and photons are rejected, where isolated leptons and photons are objects with

$$p_T^{\ell} > 10\,\text{GeV}, \quad p_T^{\gamma} > 25\,\text{GeV}, \quad |\eta| < 2.5. \tag{16}$$

The CMS collaboration performed a search in eight bins of $H_T > 275$ GeV, and found the standard

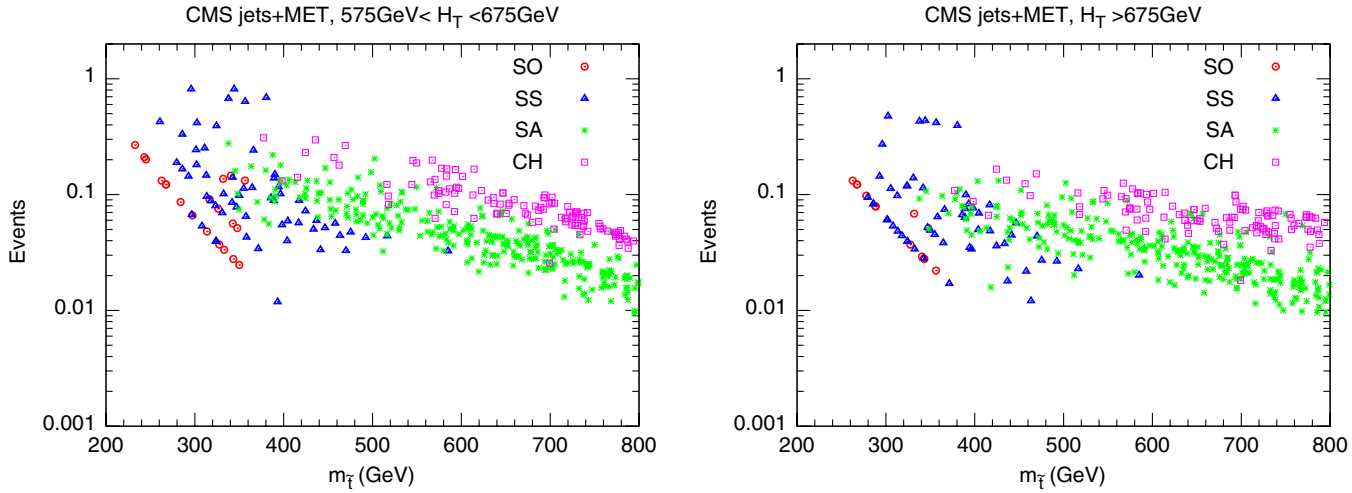

FIG. 5 (color online). The event numbers of signal in the two bins given by the CMS jets + $\not{E}_T$ searches with 575 GeV $< H_T <$ 675 GeV (left panel) and $H_T > 675$ GeV (right panel) are shown.

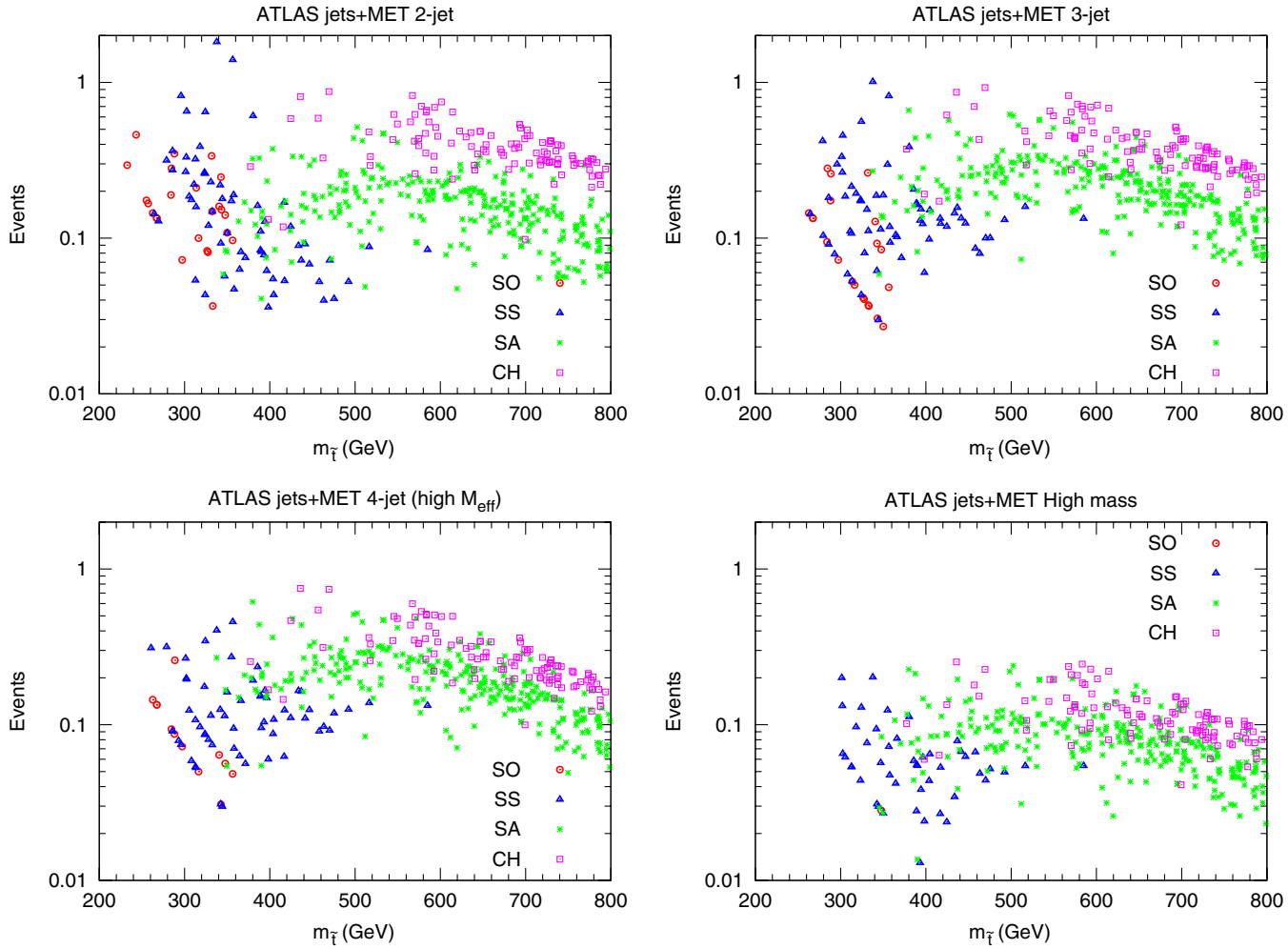

FIG. 6 (color online). The event number of signal after imposing the ATLAS 1$b$jet + jets + $\not{E}_T$ cuts: "2-jet" region (top left panel), "3-jet" region (top right panel), "4-jet high m_{eff}" region (bottom left panel), and "High-mass" region (bottom right panel), are shown, respectively.

model background per bin could fit data well. The backgrounds decrease with increasing H_T rapidly; here we consider two bins, 575 GeV $< H_T <$ 675 GeV and $H_T > 675$ GeV, in which the number of expected background is smaller than 20. We give the final event number in Fig. 5.

(ii) In Ref. [2], ATLAS takes into account the events with jets and $\not{E}_T$ with 1.04 fb^{-1} of data. Events containing muons with $p_T > 10$ GeV, $|\eta| < 2.4$ and electrons with $p_T > 20$ GeV, $|\eta| < 2.47$ are rejected. Reconstructed jets are required to satisfy

$$p_T^{j_1} > 130\,\text{GeV}, \quad p_T^{j} > 40\,\text{GeV}, \quad |\eta|_j < 2.8. \tag{17}$$

The missing transverse energy $\not{E}_T$ and the minimal $\Delta\phi(j, \not{E}_T)$ between $\not{E}_T$ and leading jets are required

$$\not{E}_T > 130\ \text{GeV}, \qquad \Delta\phi(j, \not{E}_T)_{\min} > 0.4. \tag{18}$$

To probe the SUSY parameter points with different gluino and squark masses, the collaboration define five signal regions as

A "2-jet" region, where cuts are chosen as $n_j \geq 2$, $m_{\text{eff}} > 1000$ GeV, $\not{E}_T/m_{\text{eff}} > 0.3$;

B "3-jet" region, where cuts are chosen as $n_j \geq 3$, $m_{\text{eff}} > 1000$ GeV, $\not{E}_T/m_{\text{eff}} > 0.25$;

C1 "4-jet" region, where cuts are chosen as $n_j \geq 4$, $m_{\text{eff}} > 500$ GeV, $\not{E}_T/m_{\text{eff}} > 0.4$;

C2 "4-jet" region, where cuts are chosen as $n_j \geq 4$, $m_{\text{eff}} > 1000$ GeV, $\not{E}_T/m_{\text{eff}} > 0.25$;

D "High-mass" region, where cuts are chosen as $n_j \geq 4$, $p_T^{j_{2,3,4}} > 80$ GeV, $m_{\text{eff}} > 1100$ GeV, $\not{E}_T/m_{\text{eff}} > 0.2$.

Here n_j is the number of the jets reconstructed in the event, the effective mass is the scalar sum of transverse momentum of jets and the transverse missing momentum $\not{E}_T$. The signal regions A, B, C, and D correspond to different sparticle production channels $\tilde{q}\,\tilde{q}$, $\tilde{q}\,\tilde{g}$, light-$\tilde{g}\,\tilde{g}$ and heavy-$\tilde{g}\,\tilde{g}$, respectively. We show the final event number of signal passing all cuts in Fig. 6. The excluded values of sparticle production cross section are 22 fb, 25 fb, 429 fb, 27 fb, and 17 fb, respectively.

We also implement the bounds to the stop pair events in term of cuts from the SUSY searches at LHC with 35 pb^{-1} of data. The following channels have been included in our study:

(1) CMS' jets + $\not{E}_T$ channel [71],
(2) ATLAS' jets + $\not{E}_T$ channel [72],
(3) ATLAS' 1lepton + jets + $\not{E}_T$ channel [73],
(4) ATLAS' 2leptons + jets + $\not{E}_T$ channel [74],
(5) ATLAS' 1$b$jet + jets + $\not{E}_T$ channel [75], and
(6) ATLAS' 1$b$jet + leptons + jets + $\not{E}_T$ channel [75].

For the channels containing leptons, we do not focus on the lepton sign and flavor, and sum all the allowed events together. The bounds to the event numbers of the stop pair production are shown in the Fig. 7. For these six channel, the upper limits for new physics event number set by collaborations are 13.4, 45.5, 4.7, 20.7, 10.4 and 4.7, respectively.

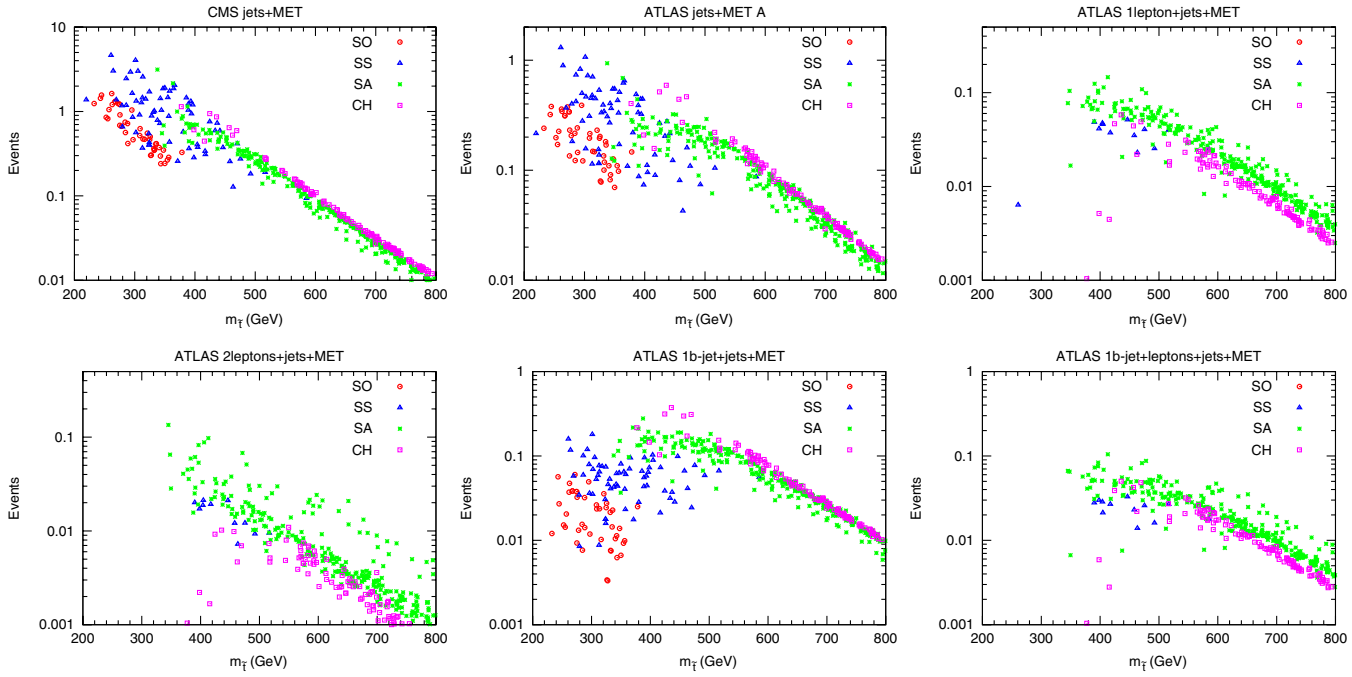

FIG. 7 (color online). The event number of signal passed all cuts from LHC searches with 35 pb^{-1} of data (from left to right and top to bottom): (1) CMS jets + $\not{E}_T$, (2) ATLAS jets + $\not{E}_T$ (signal region A), (3) ATLAS 1lepton + jets + $\not{E}_T$, (4) ATLAS 2leptons + jets + $\not{E}_T$, (5) ATLAS 1$b$jet + jets + $\not{E}_T$, and (6) ATLAS 1$b$jet + leptons + jets + $\not{E}_T$ are shown.

TABLE I. The cross sections of $pp \to \tilde{t}_1\tilde{t}_1^*$ in four benchmark points at LHC for collision energy 7 TeV and 14 TeV are presented, respectively. The masses of light sparticles (in GeV) are also given.

Benchmark points	BMP1	BMP2	BMP3	BMP4
$m_{\tilde{t}_1}$	390	243	264	338
$m_{\tilde{\tau}_1}$	207	471	199	179
$m_{\chi_1^+}$	383	424	356	337
$m_{\chi_1^0}$	206	223	190	176
σ at 7 TeV (pb)	0.23	3.74	2.33	0.55
σ at 14 TeV (pb)	2.54	28.42	18.91	5.46

When comparing the bounds from 35 pb^{-1}, we notice that the updated LHC bounds with 1 fb^{-1} of data could not further constrain those nonuniversal models allowed by the bounds from 35 pb^{-1} of data. This is simply due to the fact that these cuts are not optimized to put bounds to the light stop pair production by the experimental collaborations.

C. Benchmark points

Based on the mass pattern proposed above, we select four benchmark points (BMPs) to demonstrate their spectra and features at LHC. We tabulate the stop quark and LSP masses in Table I and provide the cross sections of these four benchmark points with the collision energy 7 TeV and 14 TeV.

We focus on the dominant decay channel of the stop, which are listed below:

BMP1: the stop dominantly decay via the $\tilde{t} \to t\chi^0$ channel (Br$(\tilde{t} \to t\chi^0) = 98.1\%$);

BMP2: the stop dominantly decay via the $\tilde{t} \to c\chi^0$ channel (Br$(\tilde{t} \to c\chi^0) = 98.7\%$);

BMP3: the stop dominantly decay via the $\tilde{t} \to b\nu_\tau\tilde{\tau} \to b\tau + \not{E}$ channel (Br$(\tilde{t} \to b\tau\not{E}) = 96.9\%$);

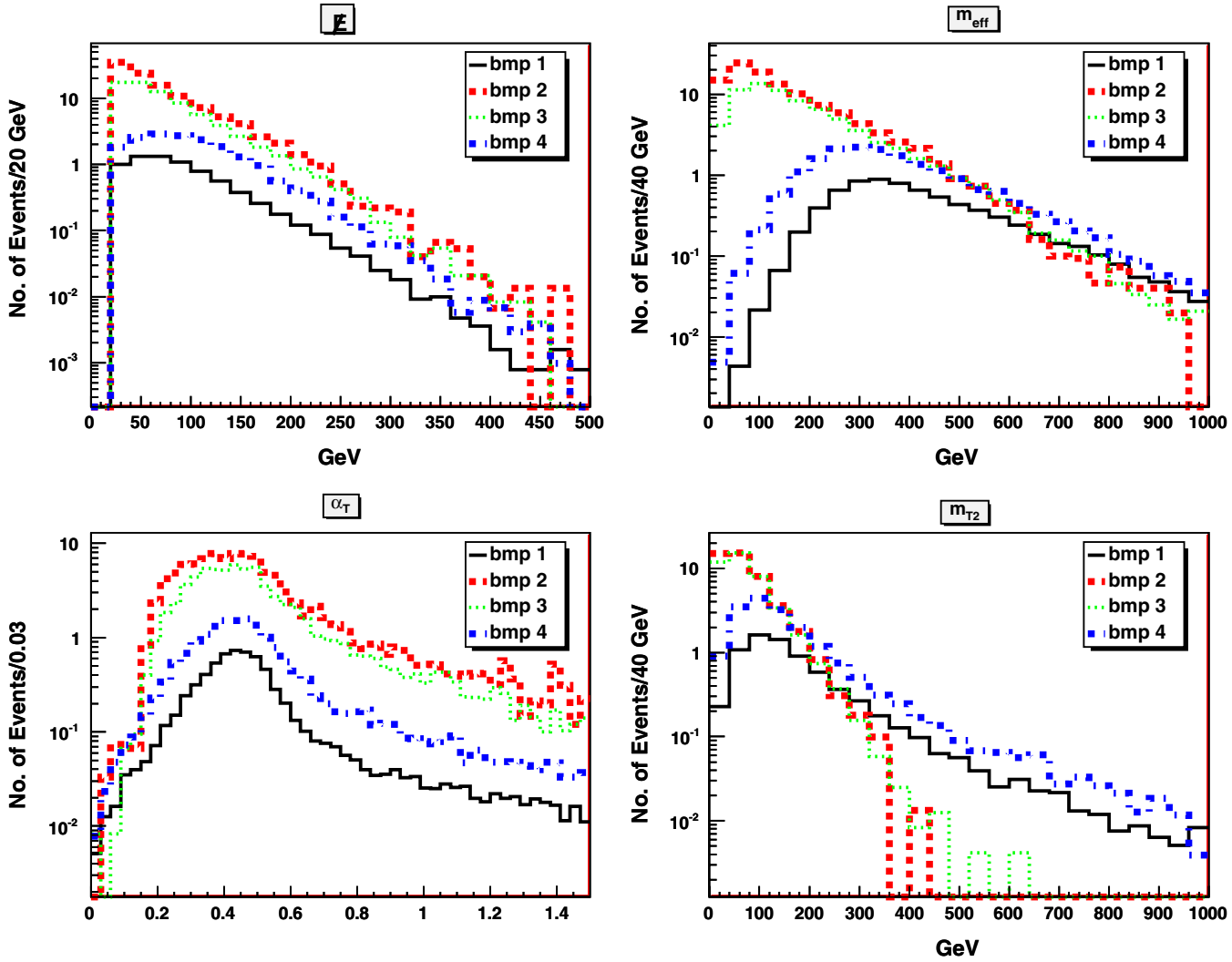

FIG. 8 (color online). The transverse missing momentum, the effective mass of the four benchmark points, the α_T and the m_{T2} quantity as well are demonstrated.

BMP4: the stop dominantly decay via the $\tilde{t} \to b$ channel ($\mathrm{Br}(\tilde{t} \to bW\chi^0) = 98.2\%$);

Below we show several salient kinematic observables for these four benchmark points in Figs. (8 and 9). These observables offer us important clues as how signal can escape the current LHC SUSY search. The distributions shown in Fig. (8 and 9) explicitly show that the current cuts of ATLAS and CMS, which are optimized for the mSUGRA search, cannot separate signal events of our benchmark points from the SM background events. There are several comments in order:

(i) The reconstructed transverse missing momentum of these benchmark points is maximal in the region with $\not{E} < 100$ GeV, as demonstrated in Fig. (8). Therefore the large missing energy cut adopted in experimental collaborations can greatly reduce the signals.

(ii) The effective mass for the benchmark point 2 and 4 is maximal in the region with $m_{\mathrm{eff}} < 300$ GeV, while for benchmark point 1 and 4 the m_{eff} can be large enough due to the large stop mass, as shown in Fig. (8).

(iii) The observables α_T and m_{T2} are shown in Fig. (8). The observable α_T is supposed to suppress QCD background heavily. Similarly, the razor method [76], which is designed to suppress the huge QCD background at LHC environment and to pick out the signal events from heavy pair-produced particles decay, cannot help to distinguish signals from these benchmark points. While the reconstructed m_{T2} observable [77] is not large for all these benchmark points, the survival rate of signal after the cut with $m_{T2} > 300$ GeV cannot be larger than 10% for benchmark point 1 and 1% for benchmark point 2, respectively.

(iv) The ratio of missing energy over H_t is shown in Fig. (9). The experimental cut on this quantity >0.3 can affect benchmark point 1 and 4 significantly.

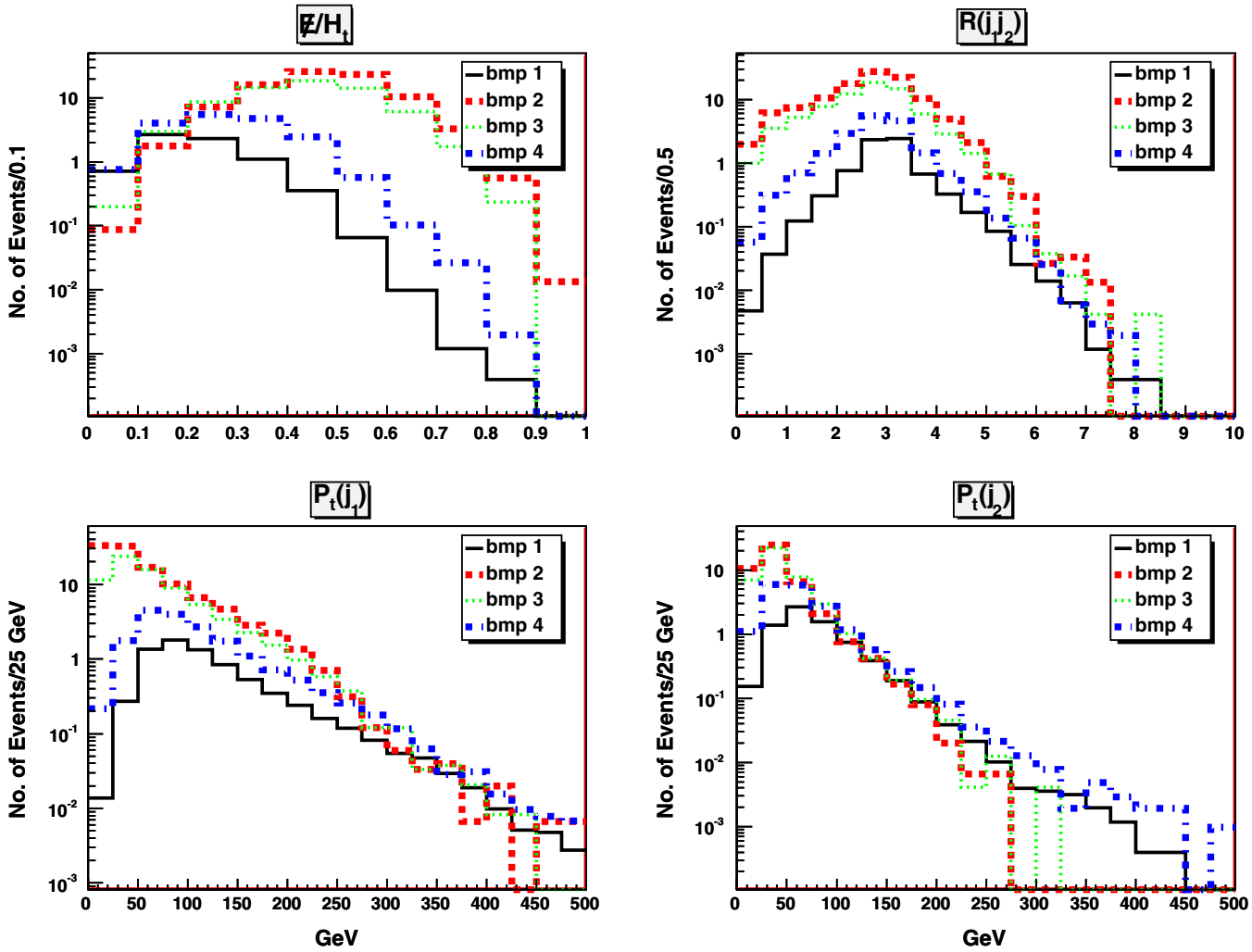

FIG. 9 (color online). The ratio of missing energy over the H_T, the angle separation of leading two jets $\Delta R(j_1, j_2)$, the transverse momentum of the leading jet, and the number of jets distribution in each benchmark point are demonstrated.

TABLE II. The percentages of lepton and jet multiplicity channels determined by our benchmark point 1 are shown.

	$2j$	$3j$	$4j$	$5j$	$\geq 6j$
$n_\ell = 0$	3%	8%	15%	16%	19%
$n_\ell = 1$	3%	7%	7%	4%	2%
$n_\ell = 2$	0.9%	0.6%	...	...	...

TABLE III. The percentages of jet multiplicity channels from the benchmark point 2.

	$2j$	$3j$	$4j$	$5j$	$\geq 6j$
$n_\ell = 0$	20%	9.5%	3.0%	1%	...

(v) The transverse momentum of the leading two jets for the benchmark point is maximal in the region with $P_t < 50$ GeV region for benchmark points 2 and 3, as demonstrated in Fig. (9). Therefore, the cut demanding the leading jet must be larger than 150 and can affect the signal significantly. Meanwhile, such a cut can also considerably reduce the signal from benchmark points 1 and 4. Similarly, the cut on the second leading jet can affect all benchmark points badly.

Next, we focus on the signature from benchmark point 1 and 2, and consider the corresponding SM backgrounds. The final states of these two benchmark points are provided in Table (II and III), where we have imposed the acceptance cuts to both of them

(1) $P_t(j) > 20$ GeV,
(2) $P_t(\ell) > 20$ GeV,
(3) $\not{E} > 20$ GeV,
(4) $\eta(j) < 2.5$, and
(5) $R(\ell, j) > 0.4$ and $R(j, j) > 0.4$ as well.

Let us first look at the signal from the first benchmark point. The search strategies for searching $\tilde{t}_1 \to t\chi^0$ can be categorized by the final states in the literature: the full-hadronic channel [78,79], the semileptonic channel [80,81], and the dileptonic channel. For the hadronic and semileptonic modes, some kinematic observables have been studied to separate the signal and background, i.e., the missing energy and effective mass. Moreover, when the tops in the final state are highly boosted, the top tagger based on the jet substructure analysis can be used to distinguish signal and background [82,83]. It is also remarkable that, due to the right-handed helicity of the light stop, the top quarks in the final state should be polarized [84]. The dileptonic channel $pp \to \tilde{t}_1\tilde{t}_1^* \to t\bar{t}\chi^0\chi^0 \to \ell\ell b\bar{b} + \not{E}$ is less studied in literature; the apparent reason is the small branching fraction. However, consider the messy background at LHC, where two leptons in the final state can help to suppress background greatly. Furthermore, in order to claim the signal is from light stop pair decay, the dileptonic channel should also be observed. So the dileptonic channel is complementary for the discover of light stop and deserves careful study.

Now, let us look at the signature of the second benchmark point. Search for the signature $\tilde{t}_1 \to c\chi_1^0$ at LHC also existed in a vast of literature. A recent work where the exact one-loop decay width for the decay of a NLSP $\tilde{t}_1$ into charm and neutralino can be found at [85]. It is remarkable that if $\tilde{t}_1$ dominantly decays into charm and neutralino, it might be quite challenging to directly detect it even though it might be copiously produced, since similar decay could occur in the T-parity little Higgs model as demonstrated in [86]. The charm jet can be very soft, which might escape the triggering; meanwhile, the reconstructed missing energy cannot be large. Therefore such events might not even be recorded. It is known that b-tagging and top-tagging can

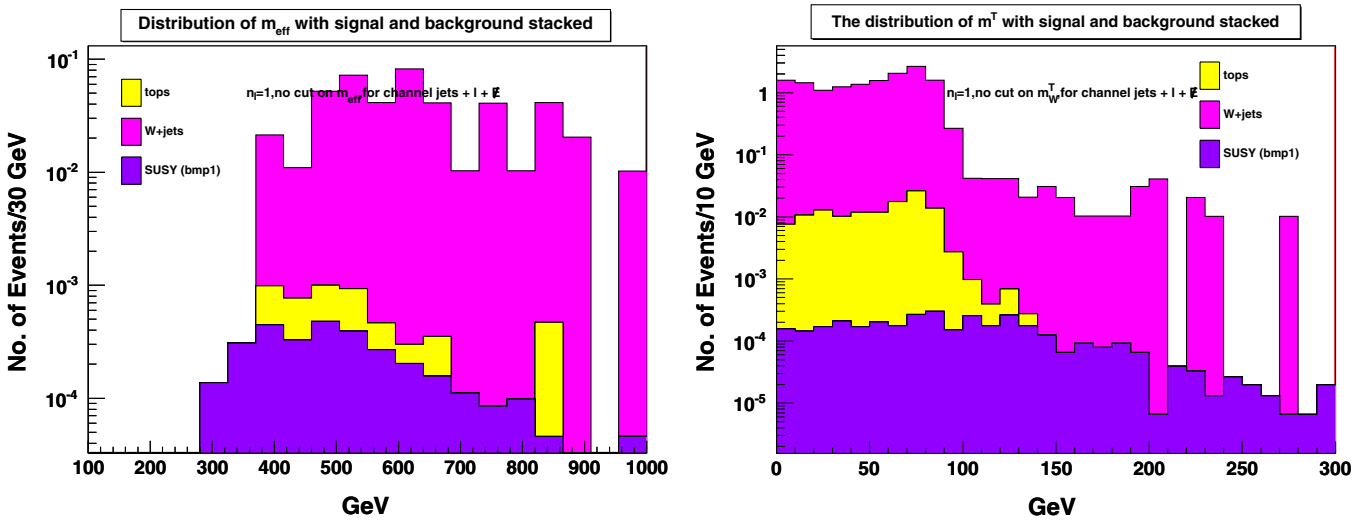

FIG. 10 (color online). The distributions of effective mass m_{eff} and the reconstructed transverse mass m^T for the channel $\not{E} + \ell +$ jets after all other ATLAS cuts for benchmark point 1 in 7 TeV are shown.

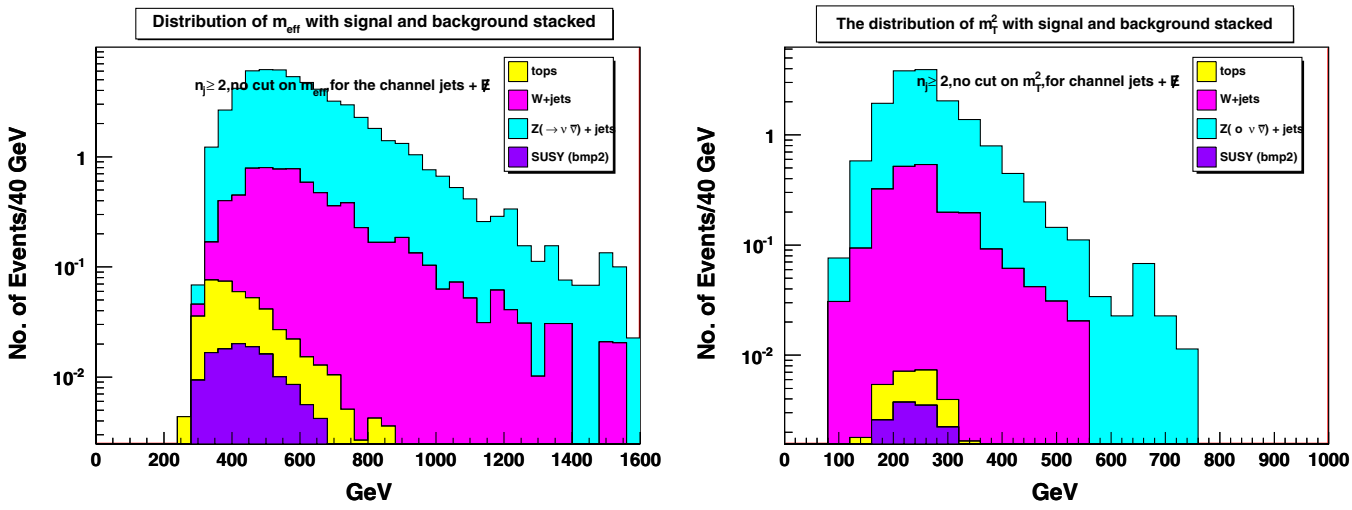

FIG. 11 (color online). The distributions of effective mass m_{eff} and the quantity m_{T2} for the channel $\not{E}$ + jets after all other CMS cuts for benchmark point 2 in 7 TeV are shown.

increase the supersymmetry signal relative the standard model backgrounds. Therefore, c-tagging techniques are also suggested to distinguish signal and QCD background [87,88].

In Fig. (10 and 11), we further show how the current ATLAS cuts and the current CMS cuts affect the observation of our benchmark points 1 and 2, respectively. The QCD background in Fig. (11) can be safely omitted due to the fact that both the α_T and R_{mis} can suppress it significantly. The plots show the distribution of the kinematic observables m_{eff} and m^T with the current ATLAS cuts and m_{T2} and m_{eff} with the current CMS cuts. After imposing all cuts, we arrive at the results given in Table IV. The results indicate that these benchmark points, especially for benchmark point 2, define a challenge to the current searching strategy. For benchmark point 1, we have studied the full-hadronic channel and the dileptonic channel (mainly suppressed by the branching fraction) and the bound from the semileptonic channel is more stringent.

Although the cross section of signal increased by a factor of 10 or so from 7 TeV to 14 TeV, the cross section of background also increased by almost the same factor. We arrive at the conclusion that, even when LHC can run with the collision energy 14 TeV, it is still challenging to explore these benchmark points.

TABLE IV. Number of events after CMS and ATLAS search cuts with integrated luminosity 35 pb^{-1} are displayed and the required luminosities with the collision energy 7 TeV for the discovery $S/\sqrt{S+B}=5$ of benchmark points 1 and 2 are estimated.

	Signal	Background	S/B	$S/\sqrt{S+B}$	Lum. (7 TeV)
BMP1	0.04	4.0 [73]	1×10^{-2}	0.02	62.5 fb^{-1}
BMP2	0.01	24.5 [71]	4×10^{-4}	0.002	6250 fb^{-1}

The signature of benchmark points 3 and 4 is $b\bar{b}\tau^+\tau^-$, where both b jets and the τs are typically soft due to the small mass splittings in the cascade decay chains. A recent study on such final states in mSUGRA context can be found in [89]. The b-tagging and tau-tagging performance with a soft b jet and a soft tau decreases which may challenge the success to distinguish signal events. Similar to the signature of benchmark points 1 and 2, the current cuts on m_{eff} and $\not{E}$ suppress the signal badly; therefore to find signature of these two benchmark points at LHC is also difficult. We neglect the detailed analysis of them.

D. Search at the ILC

The ILC is a future electron-positron collider. At the first stage, it will start with 220 GeV and run up to the maximal center of mass energy 500 GeV. At its later stages, it can be upgraded up to 1 and 3 TeV. In principle, it is also designed to be able to scan near the threshold region of particle production. Compared with hadronic collider, the ILC enjoys a much cleaner environment as well as high-energy resolution capability. For the discovery of SUSY, as one of its advantage, it can reconstruct three-dimensional momentum of missing energy.

From the ILC detectors' [90–92] design report, we take it that the energy resolution for jets is assumed as

$$\frac{\delta E}{E}=\frac{20\%}{\sqrt{E}}\oplus 1\%. \tag{19}$$

Meanwhile, since the detectors are supposed to cover the full solid angle, we assume that the coverage of detectors to charged tracks can reach to 20 for η in our fast simulation. Such a detector simulation is realized by modifying the PGS card file.

At the ILC, a pair of light stops can be produced via the s-channel γ/Z exchange. As pointed out in the design

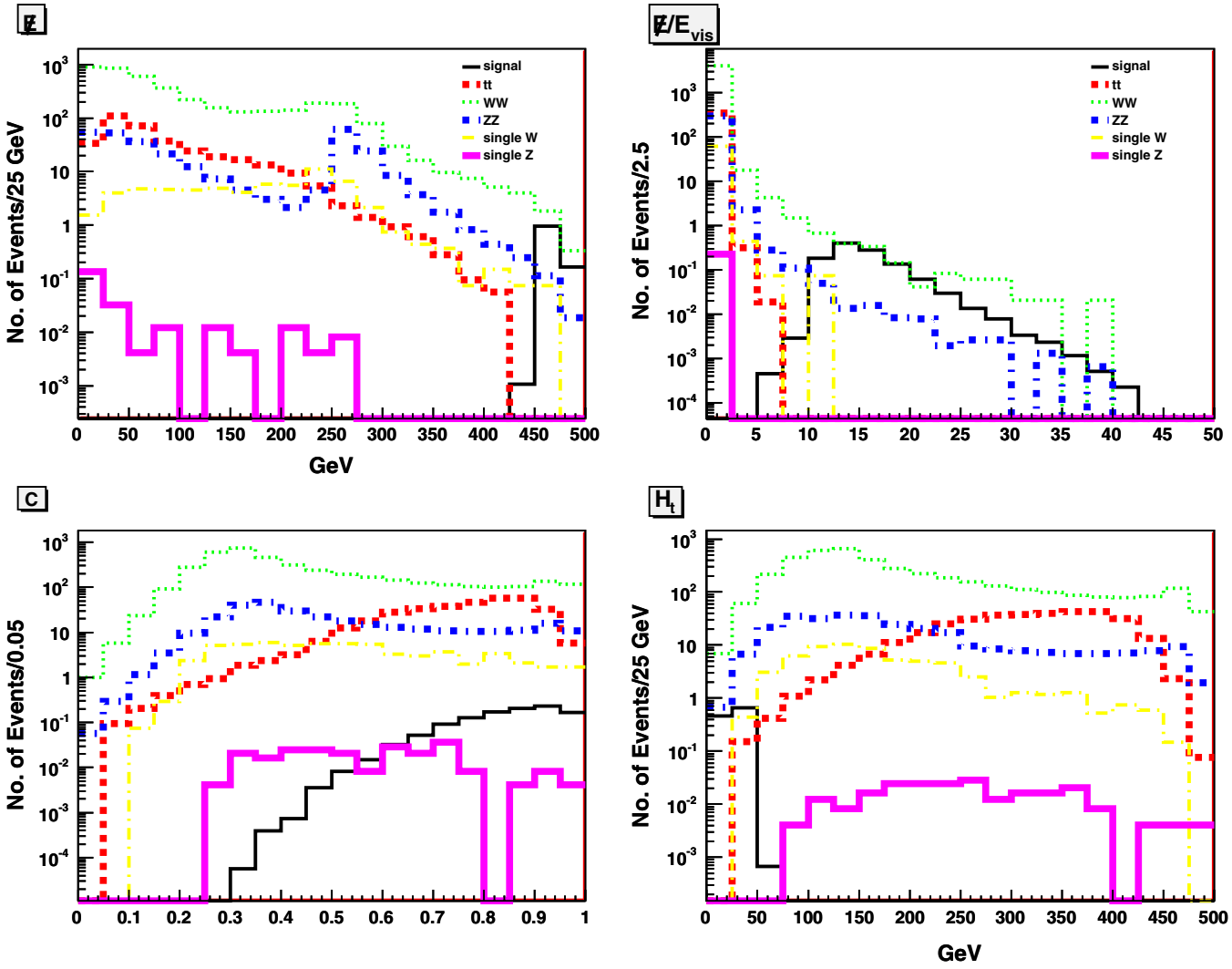

FIG. 12 (color online). The distributions of the reconstructed missing energy $\not{E}$, the ratio of $\not{E}/m_{\rm eff}$, the centrality C and the transverse momentum scalar sum H_t as well are demonstrated. The unit of the y-axis is determined by normalizing the integrated luminosity to 1 fb^{-1}.

report [93], ILC can cover the region of parameter space with the light stop. Several realistic Monte Carlo studies have been performed in the literature [94–99]. Below we focus on the detection of the signal represented by our benchmark point 2 [13].

For the benchmark point 2, the pair production of neutralinos should be possible but cannot overcome the background $e^+e^- \to \nu\bar{\nu}$. Then the light stop should be the first super particle detected at ILC. Here we update the relevant analysis by considering more kinematic observables and using the neural network discriminant to improve signal and background separation. And we find that when compared with the sequential cut method, the neural network discriminant analysis can improve both the ratio of signal over background and the significance remarkably. Our analysis can be extended to the similar study for $\tilde{b} \to b\chi^0$ and we expect the ratio of signal over background and the significance can also be considerably improved. In Figs. (12), we show the distribution of key kinematic variables used as the input of the neural network analysis, where we do not impose any a cut except the transverse momentum of jets $P_t(j) > 5$ GeV:

(i) The reconstructed missing energy $\not{E}$, which is obtained from $\sqrt{s} - E_{j_1} - E_{j_2}$. This quantity cannot be reconstructed at LHC but can be reconstructed at ILC. For signal this quantity should be large, as shown in Fig. (12), while for the background ZZ which occurs in the t and s channels, when one of Z decays invisibly, the missing energy can be around 250 Gev, thus explaining the bump in the ZZ background.

(ii) The ratio of $\not{E}/m_{\rm eff}$, where $m_{\rm eff}$ is defined as the visible energy sum of all objects in the event. Obviously, for signal, this quantity should be large,

TABLE V. The number of events (normalized to the integrated luminosity 10 fb^{-1}) after preselection, after some simple cuts and after the NN discriminant cuts are demonstrated.

	signal	$t\bar{t}$	WW	$e\bar{\nu}W$	ZZ	eeZ	S/B	$S/\sqrt{S+B}$
No. of events after preselection	11.1	6.2	336.7	8.9	44.8	$\cdots$	0.03	0.54
No. of events after a few cuts	11.1	$\cdots$	18.6	1.0	0.7	$\cdots$	0.5	1.9
No. of events after NN	9.6	$\cdots$	0.9	0.7	0.4	$\cdots$	4.8	2.6

as shown in Fig. (12). From the distribution of this quantity, it becomes quite clear that the dominant background events are from WW and ZZ.

(iii) The centrality C. In the signal, the energy tends to deposit in the direction with $\eta = 0$ region. We find this quantity is useful.

(iv) The transverse momentum scalar sum H_t and the jet mass of the two hemisphere jets. If there are more than two jets, we can use the hemisphere algorithm to group jets into two fat jets. For signal, the invariant mass of each jet should be small. While for background, like the highly boosted weak bosons, the invariant mass must be large. We find that these observables are useful to suppress background.

We can choose a few preselection rules and adopt a few simple cut methods to suppress background while maintaining a good acceptance to signal. At the preselection level, we use lepton veto and a cut on $\not{E} > 300$ GeV. Then the dominant background after preselection is WW pair and eeZ events. We also list the results in the simple cut method, where we choose: 1) $\not{E} > 425$ GeV, 2) $\not{E}/(E_{j_1} + E_{j_2}) > 10$, and 3) $m(j_1, j_2) < 60$. The results are presented in the third line of Table V. Because of the correlation among kinematic observables, it is difficult to find the best set of cuts. To finish such a task, we utilize the neural network discriminant analysis to optimize cuts. The results are presented in Table (V).

The results of the neural network discriminant are presented in the fourth line of Table V. It is obvious that the NN discriminant analysis can improve both the ratio of signal over background and the significance. From the results of the neural network analysis, we can estimate the required luminosity is 37 fb^{-1} for the discovery significance $S/\sqrt{S+B} = 5$.

A simpler version of the neural network discriminant analysis can be demonstrated in Fig. (13), where two pairs of two almost independent observables are shown. The neural network discriminant analysis basically utilizes such the correlations among observables to distinguish signal and background.

V. CONCLUSION AND DISCUSSIONS

We have studied the nonuniversal SUSY models and explored light stop pair production at the LHC. We scan the SUSY parameter space at the GUT scale and evolve to low energy, considering the bounds by LHC searches with 35 pb^{-1} and 1 fb^{-1} of data and the dark matter relic density and direct search bounds. We find that, to give

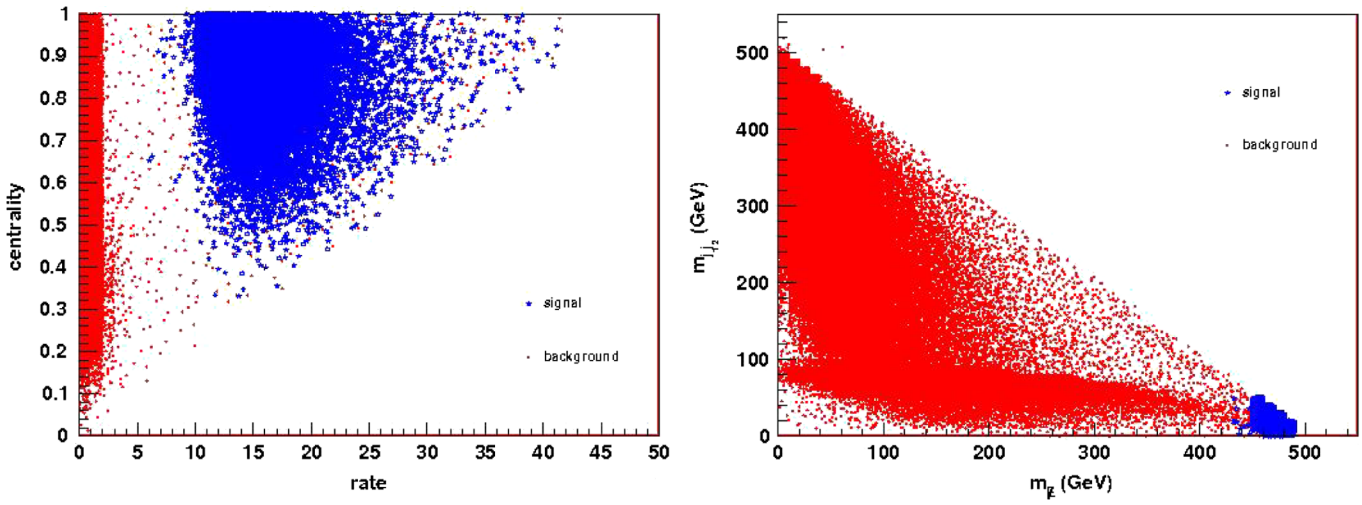

FIG. 13 (color online). Two-dimensional scatter plots for signal and background are demonstrated. The blue and red points denote signal and background, respectively. In the left panel, the correlations between the rate and centrality for signal and background is shown. In the right panel the correlation between the invariant mass of the missing 4-momentum and the invariant mass of the two leading jets is shown.

correct relic density, the stop usually has a small mass difference with neutralino. Such a scenario easily escapes the current search cuts adopted at both CMS and ATLAS collaborations.

The model we explored in the work is an important scenario, since the colored SUSY particles are the primary goal to search at LHC and gluino is usually very heavy when evolving from GUT scale to the low-energy scale. Further, we have to consider the dark matter relic density bound, at least considering the upper bound so as not to overclose the Universe. The dark matter relic density usually leads to a degenerate pattern between the light stop and the LSP neutralino.

In this work we demonstrate that it is difficult to detect the light stop scenario if only the $pp \to \tilde{t}_1\tilde{t}_1^*$ process is considered. There have been some studies to improve the ratio between signal and background using the associate production, such as via associate monojet and monophoton processes [16,100]. It is found by using the associated production that the large region of the parameter space can be covered by LHC. Another method proposed to further suppress the background is by utilizing the two energetic tagged b jets [18]. By studying the $pp \to \tilde{t}_1\tilde{t}_1^* b\bar{b}$ process [18], even the very degenerate stop neutralino scenario can be explored for LHC at 14 TeV and 500 fb^{-1} integrated luminosity.

Although the associate production channels offer a hope for detecting such a difficult scenario at LHC, the required luminosity seems too large. Our simulation shows that the ILC is an ideal place to probe these models. Whether the SUSY is hidden at LHC or SUSY does not exist at low energy may need more careful and fortitude studies.

ACKNOWLEDGMENTS

The authors thank Qing-Hong Cao, Kai Wang, C. P. Yuan and Shou-Hua Zhu for giving valuable suggestions. This work is supported by the Natural Science Foundation of China under the Grant No. 11075169 and No. 11175251, the 973 project under Grant No. 2010CB833000, and the Chinese Academy of Science under Grant No. KJCX2-EW-W01.

[1] S. Chatrchyan *et al.* (CMS Collaboration), arXiv:1109.2352.
[2] G. Aad *et al.* (ATLAS Collaboration), arXiv:1109.6572.
[3] G. L. Kane, E. Kuflik, R. Lu, and L. T. Wang, Phys. Rev. D **84**, 095004 (2011); O. Buchmueller *et al.*, Eur. Phys. J. C **71**, 1634 (2011); D. Feldman, K. Freese, P. Nath, B. D. Nelson, and G. Peim, Phys. Rev. D **84**, 015007 (2011); J. Debove, B. Fuks, and M. Klasen, Nucl. Phys. **B849**, 64 (2011); P. Athron, S. F. King, D. J. Miller, S. Moretti, and R. Nevzorov, Phys. Rev. D **84**, 055006 (2011); S. Scopel, S. Choi, N. Fornengo, and A. Bottino, Phys. Rev. D **83**, 095016 (2011); H. K. Dreiner, S. Grab, and T. Stefaniak, Phys. Rev. D **84**, 035023 (2011); B. C. Allanach, Phys. Rev. D **83**, 095019 (2011); S. Heinemeyer, Proc. Sci., KRUGER2010 (2011) 025 [arXiv:1103.0952]; B. C. Allanach, T. J. Khoo, C. G. Lester, and S. L. Williams, J. High Energy Phys. 06 (2011) 035; S. Akula, N. Chen, D. Feldman, M. Liu, Z. Liu, P. Nath, and G. Peim, Phys. Lett. B **699**, 377 (2011); J. A. Maxin, T. Li, D. V. Nanopoulos, and J. W. Walker, Phys. Rev. D **84**, 076003 (2011).
[4] H. Baer, V. Barger, and P. Huang, J. High Energy Phys. 11 (2011) 031.
[5] S. P. Martin, Phys. Rev. D **75**, 115005 (2007).
[6] T. J. LeCompte and S. P. Martin, Phys. Rev. D **84**, 015004 (2011).
[7] M. Adeel Ajaib, T. Li, Q. Shafi, and K. Wang, J. High Energy Phys. 01 (2011) 028.
[8] N. Chen, D. Feldman, Z. Liu, P. Nath, and G. Peim, Phys. Rev. D **83**, 035005 (2011).
[9] M. Adeel Ajaib, T. Li, and Q. Shafi, Phys. Lett. B **701**, 255 (2011); **705**, 87 (2011).
[10] J. M. Yang and B.-L. Young, Phys. Rev. D **62**, 115002 (2000).
[11] C. Balazs, M. S. Carena, and C. E. M. Wagner, Phys. Rev. D **70**, 015007 (2004).
[12] M. Carena, G. Nardini, M. Quiros, and C. E. M. Wagner, J. High Energy Phys. 10 (2008) 062; Nucl. Phys. **B812**, 243 (2009).
[13] M. S. Carena, A. Finch, A. Freitas, C. Milstene, H. Kluge, and A. Sopczak, Phys. Rev. D **72**, 115008 (2005).
[14] S. Kraml and A. R. Raklev, Phys. Rev. D **73**, 075002 (2006).
[15] D. Choudhury, S. K. Gupta, and B. Mukhopadhyaya, Phys. Rev. D **78**, 015023 (2008).
[16] M. Carena, A. Freitas, and C. E. M. Wagner, J. High Energy Phys. 10 (2008) 109.
[17] M. Johansen, J. Edsjo, S. Hellman, and D. Milstead, J. High Energy Phys. 08 (2010) 005.
[18] S. Bornhauser, M. Drees, S. Grab, and J. S. Kim, Phys. Rev. D **83**, 035008 (2011).
[19] I. Gogoladze, S. Raza, and Q. Shafi, Phys. Lett. B **706**, 345 (2012).
[20] Y. Kats and D. Shih, J. High Energy Phys. 08 (2011) 049.
[21] K. Huitu, L. Leinonen, and J. Laamanen, Phys. Rev. D **84**, 075021 (2011).
[22] R. Essig, E. Izaguirre, J. Kaplan, and J. G. Wacker, arXiv:1110.6443.
[23] Y. Kats, P. Meade, M. Reece, and D. Shih, arXiv:1110.6444.
[24] C. Brust, A. Katz, S. Lawrence, and R. Sundrum, arXiv:1110.6670.
[25] M. Papucci, J. T. Ruderman, and A. Weiler, arXiv:1110.6926.

[26] N. Desai and B. Mukhopadhyaya, arXiv:1111.2830.
[27] M. A. Ajaib, T. Li, and Q. Shafi, arXiv:1111.4467.
[28] J. R. Ellis, C. Kounnas, and D. V. Nanopoulos, Nucl. Phys. **B247**, 373 (1984); J. R. Ellis, K. Enqvist, D. V. Nanopoulos, and K. Tamvakis, Phys. Lett. B **155**, 381 (1985).
[29] M. Drees, Phys. Lett. B **158**, 409 (1985).
[30] T. Yanagida, Phys. Lett. B **344**, 211 (1995).
[31] N. Arkani-Hamed, H.-C. Cheng, and T. Moroi, Phys. Lett. B **387**, 529 (1996).
[32] I. Gogoladze, R. Khalid, and Q. Shafi, Phys. Rev. D **79**, 115004 (2009); **80**, 095016 (2009); I. Gogoladze, R. Khalid, S. Raza, and Q. Shafi, J. High Energy Phys. 12 (**2010**) 055.
[33] S. Dimopoulos and G. F. Giudice, Phys. Lett. B **357**, 573 (1995).
[34] A. Pomarol and D. Tommasini, Nucl. Phys. **B466**, 3 (1996).
[35] A. G. Cohen, D. B. Kaplan, and A. E. Nelson, Phys. Lett. B **388**, 588 (1996).
[36] V. D. Barger, C. Kao, and R.-J. Zhang, Phys. Lett. B **483**, 184 (2000).
[37] Y. Kawamura, H. Murayama, and M. Yamaguchi, Phys. Rev. D **51**, 1337 (1995); Phys. Lett. B **324**, 52 (1994).
[38] P. Nath and R. L. Arnowitt, Phys. Rev. D **56**, 2820 (1997); A. Corsetti and P. Nath, Phys. Rev. D **64**, 125010 (2001).
[39] N. Chamoun, C. S. Huang, C. Liu, and X. H. Wu, Nucl. Phys. **B624**, 81 (2002).
[40] D. Feldman, Z. Liu, and P. Nath, Phys. Rev. Lett. **99**, 251802 (2007); **100**, 069902 (2008)]; J. High Energy Phys. 04 (2008) 054.
[41] U. Chattopadhyay and D. P. Roy, Phys. Rev. D **68**, 033010 (2003); U. Chattopadhyay, D. Choudhury, and D. Das, Phys. Rev. D **72**, 095015 (2005); R. C. Cotta, J. S. Gainer, J. L. Hewett, and T. G. Rizzo, Nucl. Phys. B, Proc. Suppl. **194**, 133 (2009); J. Chakrabortty and A. Raychaudhuri, Phys. Lett. B **673**, 57 (2009); S. Bhattacharya, A. Datta, and B. Mukhopadhyaya, J. High Energy Phys. 10 (2007) 080; Phys. Rev. D **78**, 035011 (2008); **78**, 115018 (2008); S. P. Martin, Phys. Rev. D **79**, 095019 (2009); S. Bhattacharya and J. Chakrabortty, Phys. Rev. D **81**, 015007 (2010).
[42] S. Bhattacharya and S. Nandi, arXiv:1101.3301.
[43] R. Demina, J. D. Lykken, K. T. Matchev, and A. Nomerotski, Phys. Rev. D **62**, 035011 (2000).
[44] T. Aaltonen *et al.*, Phys. Rev. Lett. **104**, 251801 (2010).
[45] V. M. Abazov *et al.*, Phys. Lett. B **696**, 321 (2011).
[46] T. Aaltonen *et al.* (CDF Collaboration), Phys. Rev. Lett. **106**, 191801 (2011).
[47] T. Aaltonen *et al.* (CDF Collaboration), Phys. Rev. Lett. **107**, 191803 (2011).
[48] The CDF Collaboration, http://www-cdf.fnal.gov/physics/exotic/r2a/20090709.stop_charm.
[49] M. Shamim, http://lss.fnal.gov/archive/thesis/fermilab-thesis-2008-29.html.
[50] C. Boehm, A. Djouadi, and Y. Mambrini, Phys. Rev. D **61**, 095006 (2000).
[51] The CMS Collaboration, https://twiki.cern.ch/twiki/bin/view/CMSPublic/PhysicsResultsEXO11022.
[52] A. Djouadi, J. L. Kneur, and G. Moultaka, Comput. Phys. Commun. **176**, 426 (2007).
[53] D. Asner *et al.* (Heavy Flavor Averaging Group), arXiv:1010.1589.
[54] R. Aaij *et al.* the LHCb Collaboration), Phys. Lett. B **699**, 330 (2011); V. M. Abazov *et al.* (D0 Collaboration), Phys. Lett. B **693**, 539 (2010).
[55] M. Davier, A. Hoecker, B. Malaescu, and Z. Zhang, Eur. Phys. J. C **71**, 1515 (2011).
[56] K. Nakamura *et al.* (Particle Data Group), J. Phys. G **37**, 075021 (2010).
[57] D. Larson *et al.*, Astrophys. J. Suppl. Ser. **192**, 16 (2011).
[58] W. B. Lin, D. H. Huang, X. Zhang, and R. H. Brandenberger, Phys. Rev. Lett. **86**, 954 (2001).
[59] E. Aprile *et al.* (XENON100 Collaboration), Phys. Rev. Lett. **107**, 131302 (2011).
[60] G. Belanger, F. Boudjema, A. Pukhov, and A. Semenov, Comput. Phys. Commun. **176**, 367 (2007); Comput. Phys. Commun. **180**, 747 (2009); arXiv:1005.4133.
[61] G. Jungman, M. Kamionkowski, and K. Griest, Phys. Rep. **267**, 195 (1996).
[62] K. Griest and D. Seckel, Phys. Rev. D **43**, 3191 (1991).
[63] W. Beenakker, M. Kramer, T. Plehn, M. Spira, and P. M. Zerwas, Nucl. Phys. **B515**, 3 (1998).
[64] W. Beenakker, R. Hopker, and M. Spira, arXiv:hep-ph/9611232.
[65] M. Muhlleitner, A. Djouadi, and Y. Mambrini, Comput. Phys. Commun. **168**, 46 (2005).
[66] N. Bhattacharyya, A. Choudhury, and A. Datta, Phys. Rev. D **83**, 115025 (2011).
[67] J. Alwall *et al.*, J. High Energy Phys. 09 (2007) 028.
[68] T. Sjostrand, S. Mrenna, and P. Z. Skands, J. High Energy Phys. 05 (2006) 026.
[69] J. Conway *et al.* (PGS-4), conway/research/software/pgs/pgs4-general.htm.
[70] The CMS collaboration, J. Phys. G **34**, 995 (2007).
[71] V. Khachatryan *et al.* (CMS Collaboration), Phys. Lett. B **698**, 196 (2011).
[72] J. B. G. da Costa *et al.* (Atlas Collaboration), Phys. Lett. B **701**, 186 (2011).
[73] J. B. G. da Costa *et al.* (Atlas Collaboration), Phys. Rev. Lett. **106**, 131802 (2011).
[74] G. Aad *et al.* (ATLAS Collaboration), Eur. Phys. J. C **71**, 1682 (2011).
[75] G. Aad *et al.* (ATLAS Collaboration), Phys. Lett. B **701**, 398 (2011).
[76] C. Rogan, arXiv:1006.2727.
[77] C. G. Lester and D. J. Summers, Phys. Lett. B **463**, 99 (1999); A. Barr, C. Lester, and P. Stephens, J. Phys. G **29**, 2343 (2003).
[78] S. Matsumoto, M. M. Nojiri, and D. Nomura, Phys. Rev. D **75**, 055006 (2007).
[79] M. M. Nojiri and M. Takeuchi, J. High Energy Phys. 10 (2008) 025.
[80] J. Alwall, J. L. Feng, J. Kumar, and S. Su, Phys. Rev. D **81**, 114027 (2010).
[81] T. Han, R. Mahbubani, D. G. E. Walker, and L. T. E. Wang, J. High Energy Phys. 05 (2009) 117.
[82] T. Plehn, M. Spannowsky, M. Takeuchi, and D. Zerwas, J. High Energy Phys. 10 (2010) 078.
[83] T. Plehn, M. Spannowsky, and M. Takeuchi, J. High Energy Phys. 05 (2011) 135.

[84] M. Perelstein and A. Weiler, J. High Energy Phys. 03 (2009) 141.
[85] M. Muhlleitner and E. Popenda, J. High Energy Phys. 04 (2011) 095.
[86] M. S. Carena, J. Hubisz, M. Perelstein, and P. Verdier, Phys. Rev. D **75**, 091701 (2007).
[87] R. H. K. Kadala, P. G. Mercadante, J. K. Mizukoshi, and X. Tata, Eur. Phys. J. C **56**, 511 (2008).
[88] N. Bhattacharyya, A. Datta, and M. Maity, Phys. Lett. B **669**, 311 (2008).
[89] N. Bhattacharyya, A. Choudhury, and A. Datta, Phys. Rev. D **84**, 095006 (2011).
[90] T. Behnke *et al.* (ILC Collaboration), ''International Linear Collider Reference Design Report Vol. 4: Detectors,'' arXiv:0712.2356.
[91] H. Aihara *et al.* (ILD Concept Group and Linear Collider Collaboration), ''SiD Letter of Intent,'' March 2009.
[92] T. Abe *et al.* (ILD Concept Group and Linear Collider Collaboration), arXiv:1006.3396.
[93] G. Aarons *et al.* (ILC Collaboration), arXiv:0709.1893.
[94] K. i. Hikasa and M. Kobayashi, Phys. Rev. D **36**, 724 (1987).
[95] T. Han, K.-i. Hikasa, J. M. Yang, and X.-m. Zhang, Phys. Rev. D **70**, 055001 (2004).
[96] A. Bartl, W. Majerotto, K. Monig, A. N. Skachkova, and N. B. Skachkov, Phys. Part. Nucl. Lett. **6**, 181 (2009).
[97] K. Kong and S. C. Park, J. High Energy Phys. 08 (2007) 038.
[98] R. Kitano, T. Moroi, and S. f. Su, J. High Energy Phys. 12 (2002) 011.
[99] A. Arhrib and W. Hollik, J. High Energy Phys. 04 (2004) 073.
[100] N. Arkani-Hamed, S. Dimopoulos, and G. R. Dvali, Phys. Lett. B **429**, 263 (1998); G. F. Giudice, R. Rattazzi, and J. D. Wells, Nucl. Phys. **B544**, 3 (1999); J. Alwall, M. P. Le, M. Lisanti, and J. G. Wacker, Phys. Lett. B **666**, 34 (2008).